Volume 8 Number 3 2021

STUDENT JOURNAL OF PHYSICS

INTERNATIONAL JOURNAL

INDIAN ASSOCIATION OF PHYSICS TEACHERS

ISSN – 2319-3166

STUDENT JOURNAL OF PHYSICS

This is a quarterly journal published by Indian Association Of Physics Teachers. It publishes research articles contributed by Under Graduate and Post Graduate students of colleges, universities and similar teaching institutions, as principal authors.

Registered Office

Editor-in-Chief, SJP, Institute of Physics, Sainik School, Bhubaneswar, Odisha, India – 751005
(www.iopb.res.in/~sjp/)

STUDENT JOURNAL OF PHYSICS

Scope of the Journal

The journal is devoted to research carried out by students at undergraduate level. It provides a platform for the young students to explore their creativity, originality, and independence in terms of research articles which may be written in collaboration with senior scientist(s), but with a very significant contribution from the student. The articles will be judged for suitability of publication in the following two broad categories:

1. **Project based articles**
   These articles are based on research projects assigned and guided by senior scientist(s) and carried out predominantly or entirely by the student.
2. **Articles based on original ideas of student**
   These articles are originated by the student and developed by him/ her with possible help from senior advisor. Very often an undergraduate student producing original idea is unable to find a venue for its expression where it can get due attention. SJP, with its primary goal of encouraging original research at the undergraduate level provides a platform for bringing out such research works.
   It is an online journal with no cost to the author.

Since SJP is concerned with undergraduate physics education, it will occasionally also publish articles on science education written by senior physicists.

Information for Authors

- Check the accuracy of your references.
- Include the complete source information for any references cited in the abstract. (Do not cite reference numbers in the abstract.)
- Number references in text consecutively, starting with [1].

- Language: Papers should have a clear presentation written in good English. Use a spell checker.

Submission

1. Use the link "Submit" of Website to submit all files (manuscript and figures) together in the submission (either as a single .tar file or as multiple files)
2. Choose one of the Editors in the link "Submit" of Website as communicating editor while submitting your manuscript.

Preparation for Submission

Use the template available at "Submit" section of Website for preparation of the manuscript.

Re-Submission

- For re-submission, please respond to the major points of the criticism raised by the referees.
- If your paper is accepted, please check the proofs carefully.

Scope

- SJP covers all areas of applied, fundamental, and interdisciplinary physics research.

The Argument for a Low Energy Steady State Solar Neutron Flux

Zoe Marzouk[1,2], Nicole Benker[2,3]
[1] Senior undergraduate, B. Sc., Department of Mechanical and Materials Engineering, University of Nebraska, Walter Scott Engineering Center, Lincoln NE 68588-0656, U. S. A.
[2] Department of Physics and Astronomy, Theodore Jorgensen Hall, 855 North 16th Street, University of Nebraska-Lincoln, Lincoln, NE 68588-0299, U. S. A.
[3] Recent B. Sc. in physics, University of Nebraska - Lincoln; now staff with the Pacific Northwest National Laboratory, 902 Battelle Boulevard, P.O. Box 999, Richland WA 99352, U. S. A.

Abstract: Recent experiments have suggested that there is a low energy solar neutron flux. Findings from the DANSON solar neutron detector experiment, which took data from October of 2016 to March of 2017, are revisited to provide a context for this suggested solar neutron flux. The fraction of neutrons arriving at 1 au (astronomical unit) has been calculated and used to determine the possible neutrino flux from the beta decay of the low energy solar neutron flux. Because there has been solar flare data reported during the time of this experiment, solar events cannot be ruled out as the source of this flux. Here we present an analysis that indicates the need for a comparison of data from an earth-based neutrino detector and for more experiments with real-time neutrino detectors and real-time neutron spectroscopy in low Earth orbit.

Keywords: Helio astronomy, solar neutrons, neutron decay

1. INTRODUCTION

Several experiments, e.g. MESSENGER [1,2] and DANSON [3], have now suggested that there is a low energy solar neutron flux, though this is not without controversy [4]. MESSENGER experienced higher than expected neutron counts from low energy neutrons during solar flare events, suggesting a low energy neutron flux from the sun [1,2]. The Comptel detector [5], although primarily a gamma ray detector, also detected significant neutrons but only above 8 MeV, which is higher than the neutron energies from the MESSENGER [1,2] and DANSON [3] detectors. The Comptel detector did detect solar neutrons but observed solar neutrons only in bursts associated with solar flares [6-12]. Though there is evidence for a low energy solar neutron flux, it is uncertain whether such neutrons are steady state (uniform over time) or associated with shorter bursts.

A multi-layer neutron detector designed to act as a neutron calorimeter, the DANSON detector [3], was launched and deployed aboard the International Space Station, collecting data over $8x10^6$ seconds. Effectively, the DANSON detector was a passive neutron calorimeter or spectrometer, so as to roughly determine the possible low-energy solar neutron flux and approximate mean energy of neutrons below 10 MeV [3].

The high energy solar neutron flux is produced by solar flares and other events that have been documented [8-25] and understood. The origin of the observed low energy solar neutron flux, observed by DANSON and MESSENGER [1-3] is, however, not known. So learning whether observed low energy solar neutron flux (less than 10 MeV) is steady state resulting from solar nucleosynthetic processes or associated with solar coronal mass discharge events will aid in the study of the phenomenon.

2. THE MEAN ENERGY FOR THE LOW ENERGY SOLAR NEUTRON FLUX

While the MESSENGER experiment placed the low energy neutron flux between 1 and 10 MeV, DANSON refined the low energy neutron flux to be in the region of 2 to 4 MeV. To further refine this estimate, the data collected during DANSON's operation was compared to the expected neutron energy distribution among the layers determined by Monte Carlo simulation provided previously to model DANSON [3]. It is realistic to expect that cosmic ray created neutrons and backscattered neutron would enter the DANSON detector from the earth facing (nadir side) of the detector. Such neutrons, not of solar origin, could contribute counts at the DANSON detector layer where solar neutrons would exit the detector. These additional non-solar neutron counts were not part of the Monte Carlo simulation [3] and there is some indication in the DANSON data of "extra" neutrons entering the DANSON detector from the nadir side. Accordingly, the data from the nadir side of the detector, in the data reported for DANSON [3], was excluded from the fit to reduce complications from backscattered neutrons that might not be part of the direct low energy solar neutron flux. For each incident energy in Figure 1, the squares of the difference between the expected capture at each layer and actual capture at each detector layer, each as fractions of the maximum value of each curve, were totaled for each incident energy. The lowest value for the difference between expected data and the data collected shows the incident energy for the neutrons, which was found to be about 2 MeV.

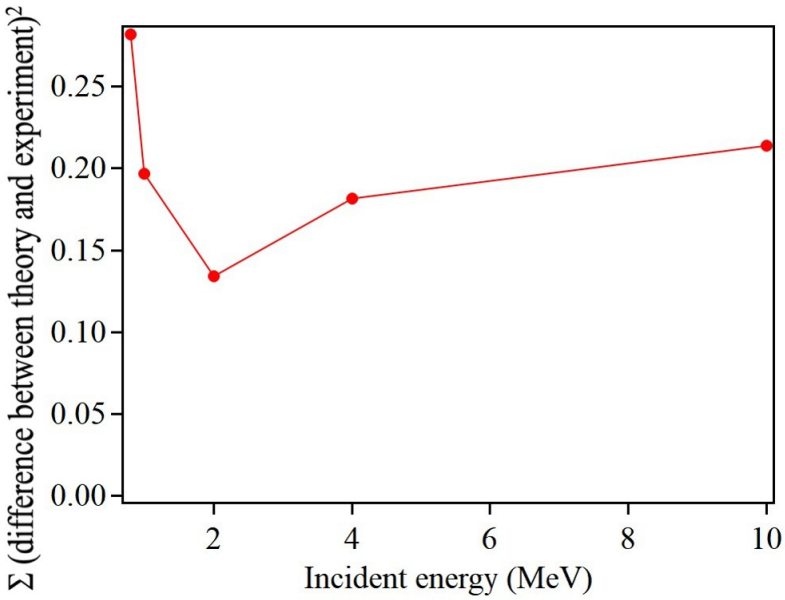

Figure 1: The experimental layer by layer detector response is compared to the simulation for DANSON detector response at that neutron energy. The sum of the square of the difference between experimental measurement of neutron intensity from DANSON data and the expected value of neutron intensity determined by Monte Carlo simulation [3], as a fraction of total counts.

Knowing the energy, the time it takes for neutrons to get to Earth can be calculated. This calculation can be used to determine the fraction of neutrons that arrive at 1 au based on standard neutron decay time which lies between 879.6±0.8 [26,27] and 885.7 ± 0.8 [28] seconds. This detectable fraction of solar neutrons at low energy, at 1 au, is a very small fraction of the initial neutron flux. At a neutron energy of 2 MeV, the fraction of neutrons arriving at the detector is 1.705×10^{-4}. The decay of most solar neutrons of low kinetic energy, at 1 au, means an increase in the solar neutrino flux, since the neutrons of 2 MeV mean energy, detected by the DANSON experiment, will have mostly decayed into a proton, an electron, and an electron antineutrino. This is caused by the conversion of the negatively charged (−1/3 e) down quark to the positively charged (+2/3 e) up quark by emission of a weak force W^- boson which decays into an electron and an electron antineutrino, i.e. $n \rightarrow p + e^- + \bar{\nu}_e$. The fraction of neutrons that arrive at 1 au also determines the fraction that have decayed before 1 au.

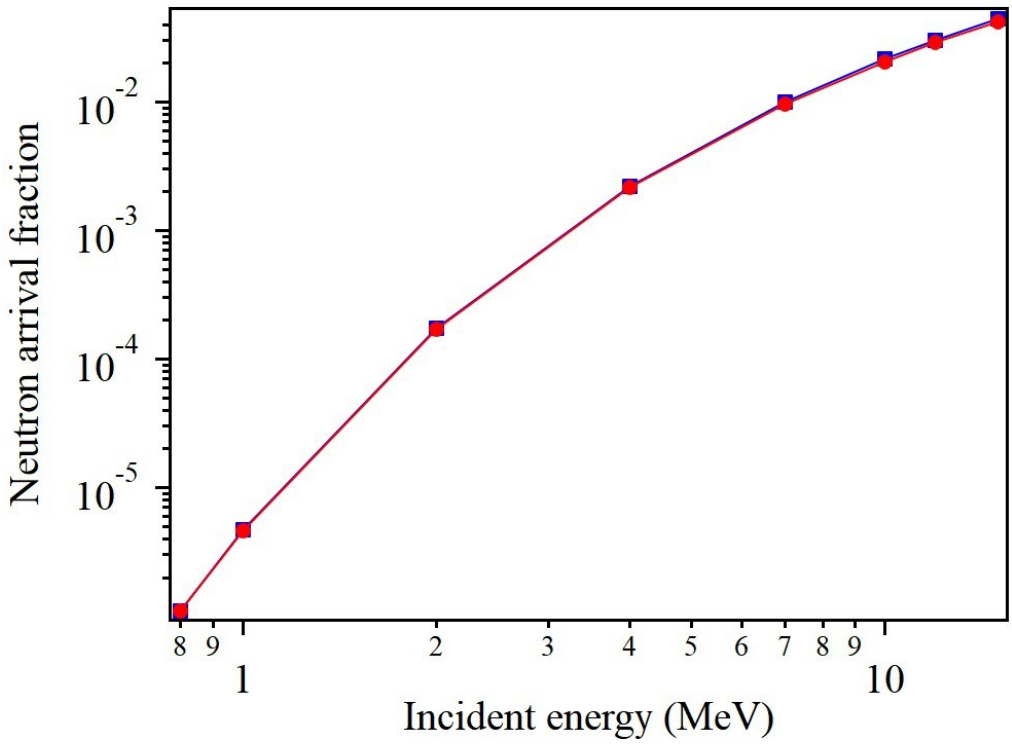

Figure 2: The calculated fraction of solar neutrons arriving at 1 au using the expected neutron decay lifetime (red) and using the decay lifetime with relativistic correction (blue).The relativistic correction to the decay lifetime for low-energy neutrons are small, becoming relevant only at higher neutron energies.

3. NEUTRINO FLUX FROM LOW-ENERGY SOLAR NEUTRONS

Since it was determined [3] that 250-375 neutrons·cm^{-2}s^{-1} arrive at 1 au, the number of antineutrinos generated by the neutron decay can be calculated. Over a period of 8x10^{6} seconds, the total number of neutrinos will be roughly 3.4x10^{12} as a result of the decay of the vast majority low energy solar neutrons that do not reach 1 au. If this additional neutrino flux was divided into two or three short bursts over that length of time, each short burst would contain 10^{11} to 10^{12} neutrinos·cm^{-2}s^{-1}. Not all of these electron antineutrinos will arrive at an earth-based neutrino detector; additionally, the generated neutrinos will not necessarily move in the direction of the neutron flux. The neutrino flux, generated by the beta decay of the low kinetic energy solar neutron flux, may still be large enough that a short burst of neutrinos would be detected by one or more of the current neutrino detectors.

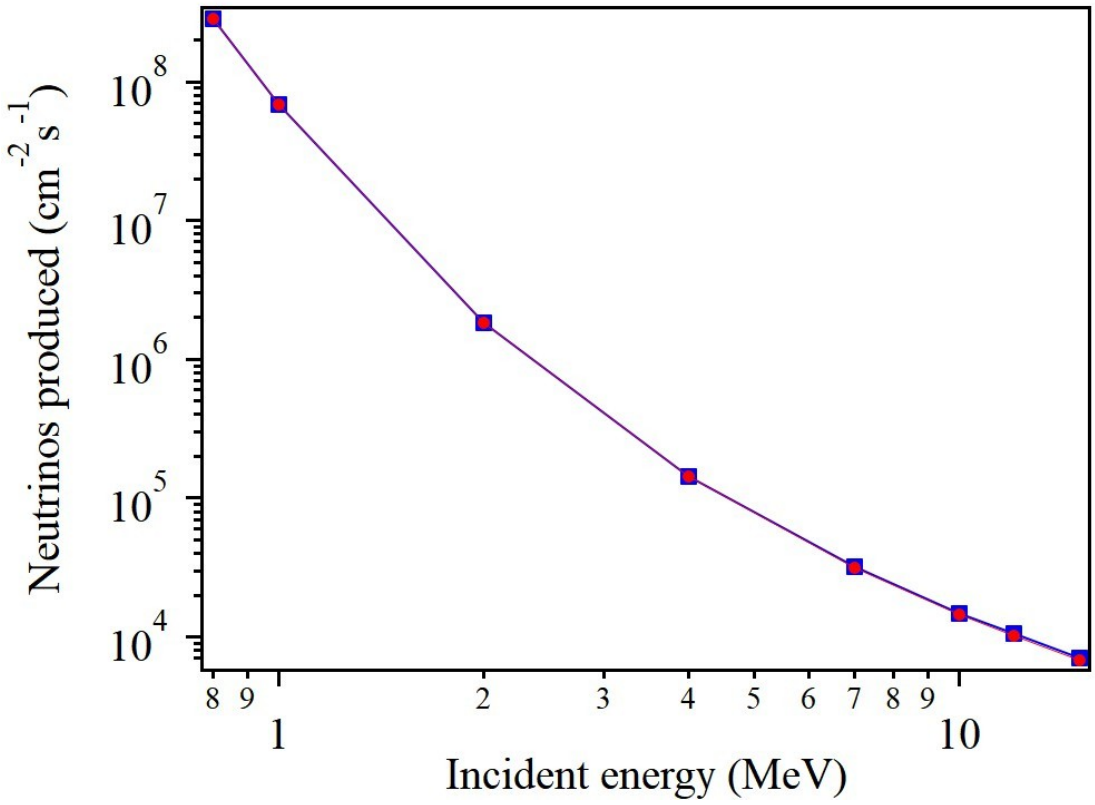

Figure 3: The expected neutrino flux from solar neutron decay (see text) calculated from Figure 2 both with (red) and without (blue) relativistic correction.

4. DISCUSSION

In order to assess the likelihood of a steady state solar neutron flux of around 2 MeV mean energy, it must be known whether there was solar activity recorded during the time of DANSON's operation. NOAA recorded some solar activity during that time from late 2016 to early 2017 [26]. This has to be a serious consideration because solar flare events between October 23, 2016 to March 17, 2017 would coincide with the period of neutron data collection by DANSON [3]. Because there was solar activity, it must be considered that DANSON's neutron capture signal may include neutrons from these solar flare events. In the case that solar flares contributed to this neutron count, it is important to note that the flares would have to be of significantly low energy, around 1 to 4 MeV, as compared to more familiar high energy flares of energies around 75 MeV [8,9,11-13,15,16,18-20,23], because of the low-energy acceptance window of the DANSON detector [3].

The relation of these known solar flare events [29] to DANSON's neutron capture count could be established by comparison with real-time neutrino detectors to see if there was an increase in neutrinos associated with the decay 2 to 4 MeV energy solar neutrons at the times of solar flares. The main contribution to the solar neutrino flux comes from the proton-proton reaction, with a peak flux above 10^{11} neutrinos $cm^{-2}*sec^{-1}$ at 1 au, and these neutrinos have a low energy, up to 400 keV [20-33], thus would overlap with the antineutrino flux resulting from neutron beta decay, which would also be at energies below 1 MeV. There are many neutrino detectors, including Sanford Underground Research Facility (SURF), Borexino, San Grasso, Super Kamiokande, Sudbury, and still others [30,31]. Each of these detectors has a different sensitivity to the neutrino that can be detected. Not all are sensitive to electron antineutrinos and furthermore, previous experiments sensitive to low energy neutrinos (SAGE, Gallex, GNO) did not measure the individual fluxes [31], unlike Borexino [34]. In this regard, the Borexino neutrino detector is of interest for comparison because this is one of the few neutrino detectors that is sensitive to the inverse beta decay reaction channel, and hence electron antineutrinos [35], with some detection sensitivity to neutrino energies below 1 MeV [32,34,36].

A neutrino flux that occurs from the decay of steady state neutron flux would be difficult to detect over the solar neutrino background produced by the proton-proton solar neutrino production mechanism, since the added neutrino flux would be orders of magnitude below this solar neutrino flux of solar origin which, as noted above, is in the region of 10^{11} neutrinos $cm^{-2}*sec^{-1}$ at 1 au). In contrast, if the neutrons came in two or three short bursts over the data collection period of the DANSON detector, then the neutrino flux measured by Borexino and other neutrino detectors might experience a significant, noticeable increase during the solar flare events, since only then would the neutrino production, from the decay of neutrons, be in bursts on or above the order of magnitude of the solar background produced by the proton-proton neutrino signal.

Detection of a possible neutrino flux, generated by the beta decay of the low kinetic energy solar neutron flux, will be complicated by the fact that while such neutrinos would be low-energy, neutrinos created from the decay of low kinetic energy solar neutron will be spread over a significant energy window. The significant energy window of the neutrino energy is required because the kinetic energy distribution of beta particles, resulting from beta decay, are diffuse, or roughly continuous [37-39], although decreasing in intensity up to 1 MeV. Such neutrinos will thus have an energy spectrum difficult to distinguish from the neutrinos created by the proton-proton mechanism.

If no neutrino bursts of energy less than 1 MeV have been reported or detected by the Borexino Collaboration or any other neutrino detector project, this would diminish the likelihood that the 1 to 4 MeV low energy solar neutron flux arrives in bursts. Yet an absence of detected neutrino bursts at energies below 1 MeV, correlated with solar flare events, does not exclude the possibility of antineutrino bursts resulting from the decay of episodic low energy solar neutrons, as detected by DANSON [3].

5. CONCLUSION

There is now a need to compare the recorded solar activity, specifically the solar flare events between October 23, 2016 to March 17, 2017, to any sudden influx of neutrinos captured by a real-time neutrino detector like Borexino, at neutrino energies below 1 MeV. Alternatively, a real time neutron detector with greater sensitivity to neutrons at lower energies could also be used to clarify the origin of low-energy solar neutrons. Such a real time neutron detector would provide the capability to compare the solar neutron flux to solar flare events. With real time data, the solar neutron flux could be monitored to measure for bursts or steady state flux and more accurately measure the energy of the flux. Determining the nature of the solar neutron flux, whether it is steady state or not, would lead to answers about the origin of these low-energy neutrons. If the neutrino detector efficiencies are improved sufficiently, such a neutron detector would also permit a comparison of the low energy neutron flux and the solar neutrino flux in real time.

If the production of the low energy solar neutron flux is largely steady state, then long sought measurements of the quadrupolar moment of the sun may be possible [40-43]. This latter measurement could be significant because an accurate determination of the quadrupolar moment of the sun could providing new insights into the cosmological constant [43-45].

6. ACKNOWLEDGEMENTS

This research was funded by the by Nebraska Public Power District through the Nebraska Center for Energy Sciences Research, the University of Nebraska UCARE program and the Nebraska MRSEC (DMR-1420645). The authors would like to acknowledge the guidance of Dr. Peter Dowben for his consistent support throughout the project.

REFERENCES

[1] W. C. Feldman, D. J. Lawrence, J. O. Goldsten, R. E. Gold, D. N. Baker, D. K. Haggerty, G. C. Ho, S. Krucker, R. P. Lin, R. A. Mewaldt, R. J. Murphy, L. R. Nittler, E. A. Rhodes, J. A. Slavin, S. C. Solomon, R. D. Starr, F. Vilas, and A. Vourlidas, *J. Geophys. Res.: Space Physics*, **115**(A1), A01102 (2010); doi: 10.1029/2009JA014535

[2] D. J. Lawrence, W. C. Feldman, J. O. Goldsten, P. N. Peplowski, D. J. Rodgers, S. C. Solomon, *J. Geophys. Res.: Space Physics* **119**, 5150S (2014); doi: 10.1002/2013JA019037

[3] N. Benker, E. Echeverria, R. Olesen, B. Kananen, J. McClory, Y. Burak, V. Adamiv, I. Teslyuk, G. Peterson, B. Bradley, E. R. Wilson, J. Petrosky, B. Dong, J. Kelber, J. Hamblin, J. Doumani, P. A. Dowben, and A. Enders, *Radiation Measurements* **129,** 106190 (2019); doi: 10.1016/j.radmeas.2019.106190

[4] G. H. Share, R. J. Murphy, A. J. Tylka, B. R. Dennis, and J. M. Ryan. *J. Geophys. Res.: Space Physics*, **120**, 1 (2014); doi: 10.1002/2014JA020663

[5] V. Schoenfelder, H. Aarts, K. Bennett, H. DeBoer, J. Clear, W. Collmar, A. Connors, A. Deerenberg, R. Diehl, A. von Dordrecht, J. W. den Herder, W. Hermsen, M. Kippen, L. Kuiper, G. Lichti, J. Lockwood, J. Macri, M. McConnell, D. Morris, R. Much, J. Ryan, G. Simpson, M. Snelling, G. Stacy, H. Steinle, A. Strong, B. N. Swanenberg, B. Taylor, C. deVries, and C. Winkler. *Astrophys. J. Suppl. Ser.* **86**, 657 (1993); doi: 10.1086/191794

[6] J. Ryan, K. Bennett, H. Debrunner, D. Forrest, J. Lockwood, M. Loomis, M. McConnell, D. Morris, V. Schönfelder, B. N. Swanenburg, and W. Webber. *Advances in Space Research* **13**, 255-258 (1993).

[7] D. J. Morris, H. Aarts, K. Bennett, J. A. Lockwood, M. L. McConnell, J. M. Ryan, V. Schönfelder, H. Steinle, and X. Peng. *J. Geophys. Res.* **100**, 12243 - 12249 (1995).

[8] McConnell, M. McConnell, Bennett, K. Bennett, Forrest, D. Forrest, Hanlon, L. Hanlon, Ryan, J. Ryan, Schönfelder, V. Schoenfelder, Swanenburg, B. N. Swanenburg, Winkler, and C. Winkler. *Advances in Space Research* **13**, 245 (1993); doi: 10.1016/0273-1177(93)90485-T.

[9] M. McConnell in: *High-Energy Solar Phenomena—A New Era of Spacecraft Measurements,* J. M. Ryan and W. T. Vestramd, eds., AIP Conf. Proc. **294**, 21 (1994); doi: 10.1063/1.45193

[10] J. M. Ryan. *Space Science Reviews*, **93**, 581 (2000); doi:10.1023/A:1026547513730

[11J. M. Ryan, D. Forrest, J. Lockwood, M. Loomis, M. McConnell, D. Morris, and W. Webber. in: *High-Energy Solar Phenomena—A New Era of Spacecraft Measurements,* J. M. Ryan and W. T. Vestramd, eds., AIP Conf. Proc. **294**, 89 (1994); doi: 10.1063/1.45205

[12] J. M. Ryan, and M. M. McConnell in: *High energy solar physics,* AIP Conf. Proc. **374**, 200 (1996); doi: 10.1023/A:1026547513730

[13] E. L. Chupp, D. J. Forrest, J. M. Ryan, J. Heslin, C. Reppin, K. Pinkau, G. Kanbach, E. Rieger, and G.H. Share. *Astrophys. J.*, **263**, L95 (1982); doi: 10.1086/183931

[14] G.D. Holman, *Particle Acceleration in Large-Scale DC Electric Fields*. ASP Conf. Ser., R. Ramaty, N. Mandzhavidze, eds., Astron. Soc. Pac, **206**, 135 (2000).

[15] S.N. Kuznetsov, V. G. Kurt, B. Myagkova, B. Y. Yushkov, and K. Kudela. *Solar System Research*, **40**, 104 (2006); doi: 10.1134/S0038094606020031

[16] S. N. Kuznetsov, V. Kurt, B. Y, Yushkov, K. Kudela, and V. I. Galkin. *Sol. Phys.*, **268**, 175 (2011); doi: 10.1007/s11207-010-9669-2

[17] S. Masuda, T. Kosugi, H. Hara, S. Tsuneta, and Y. Ogawara. *Nature*, **371**, 495 (1994)

[18] Y. Muraki and S. Shibata in: *High energy solar physics,* AIP Conf. Proc., **374**, 256 (1996); doi: 10.1063/1.50961

[19] Y. Muraki, K. Koga, T. Goka, H. Matsumoto, T. Obara, O. Okudaira, S. Shibata, and T. Yamamoto. *Advances in Astronomy*, **2012**, 379304 (2012); doi: 10.1155/2012/379304

[20] R. J. Murphy, G. H. Share, K. W. DelSignore, and X.-M. Hua. *Astrophys. J.*, **510**, 1011 (1999); doi: 0004-637X/510/2/1011

[21] H.E. Petschek. Magnetic Field Annihilation. in *Proc. AAS-NASA Symp*, W. N. Hess, ed., **50**, 425 (1964).

[22] G. Rank, K. Bennett, H. Bloemen, and H. Debrunner in: *High Energy Solar* Physics. AIP Conf. Proc. **374**, 219

[23] M. A. Shea, D. F. Smart, K. R. Pyle. *Geophys. Res. Lett.*, **18**, 1655 (1991).

[24] K. Shibata. *Astrophysics and Space Science*, **264**, 129 (1998); doi: 10.1023/A:1002413214356

[25] T. Yokoyama, and K. Shibata. *Astrophys. J.,* **494**, L113 (1998); doi: 10.1086/311174

[26] F.E. Wietfeldt and G.L. Greene, Reviews of Modern Physics 83 1173 (2011); doi: 10.1103/RevModPhys.83.1173.

[27] P.A. Zyla et al. (Particle Data Group), Prog. Theor. Exp. Phys. **2020**, 083C01 (2020); doi: 10.1093/ptep/ptaa104

[28] W.-M. Yao et al. (Particle Data Group), *J. Phys. G* **33**, 1 (2006); doi: 10.1088/0954-3899/33/1/001.

[29] National Oceanic Atmospheric Administration. *Solar h-alpha flare events* [Data set]. National Centers for Environmental Information (2016). URL: https://www.ngdc.noaa.gov/stp/space-weather/solar-data/solar-features/solar-flares/h-alpha/reports/soon/halpha-flare-report_soon_2016.txt

[30] A. Bellerive, *International Journal of Modern Physics A* **19**, 1167–1179 (2004); doi: 10.1142/S0217751X04019093

[31] W. C. Haxton, R. G. Hamish Robertson, and A. M. Serenelli, *Annual Review of Astronomy and Astrophysics* **51**, 21-61 (2013); doi: 10.1146/annurev-astro-081811-125539

[32] J. N. Bahcall, C. Pena-Garay, *New J. Phys.* **6**, 63 (2004); doi: 10.1088/1367-2630/6/1/063

[33] J. N. Bahcall, M. H. Pinsonneault, *Phys. Rev. Lett.* **92**, 121301 (2004); doi: 10.1103/PhysRevLett.92.121301

[34] G. Bellini et al. (Borexino Collaboration), *Phys. Lett. B* **687**, 299–304 (2010); doi: 10.1016/j.physletb.2010.03.051

[35] G. Bellini et al. (Borexino Collaboration), *Phys. Rev. Lett.* **108**, 051302 (2012); doi: 10.1103/PhysRevLett.108.051302

[36] M. Agostini et al. (Borexino Collaboration), *Phys. Rev. D* **100**, 082004 (2019); doi: 10.1103/PhysRevD.100.082004

[37] J. Chadwick, *Verhandlungen der Deutschen Physikalischen Gesellschaft* **16**, 383–391 (1914).

[38] L. M. Brown, *Physics Today* **31**, 23–8 (1978); doi: 10.1063/1.2995181.

[39] G. J. Neary, *Roy. Phys. Soc. (London) A* **175**, 71 (1940).

[40] R. H. Dicke, *Science* **184,** 419-429 (1974); doi: 10.1126/science.184.4135.419

[41] R. H. Dicke, H. M. Goldenberg, *Astrophys. J. Suppl.* **27**, 131-182 (1974).

[42] R. H. Dicke, J. R. Kuhn, K. G. Libbrecht, *Nature* **316**, 687 (1985).

[43] D. O. Gough, *Nature* **298**, 334–339 (1982)

[44] S. M. Carroll, Spacetime and Geometry (Pearson/Addison Wesley). pp. 300–307 (2004). ISBN 978-0805387322.

[45] A. Ashtekar, B. Bonga, A. Kesavan, *Phys. Rev. D* **92**, 104032 (2015); doi: 10.1103/PhysRevD.92.104032

Equivalence of Tensor Product and Partner Hamiltonian Formalism in Supersymmetric Quantum Mechanics

Rathindra Nath Das[1†] **and Archana Maji**[1 ‡]
[1]4th semester, M.Sc., Department of Physics, Indian Institute of Technology Bombay, Powai, Mumbai - 400076, India

Abstract. In this article we first write a brief review of supersymmetric quantum mechanics and then we discuss the equivalence of two co-existing formalisms viz. tensor product formalism and partner hamiltonian formalism for 1-D SUSY harmonic oscillator. We also present a Mathematica code with which one can calculate the eigenstates of any 1-D SUSY partner Hamiltonian along with two illustrated examples of 1-D SUSY harmonic oscillator and 1-D SUSY infinite potential box. Then we calculate the SUSY partner wave function for 1-D anharmonic oscillator using this code and plot first few of them. Finally, we give an example how the supersymmetric partner potentials can be calculated starting from a well-behaved ground state wave function [1].

Keywords. Supersymmetry , elementary particles , equivalence of formalisms , quantum mechanics

1. SUPERSYMMERIC QUANTUM MECHANICS

The promising idea of supersymmetry in physics started becoming the point of attraction in the late twenties. The main idea here is to consider a broader picture of the standard model in particle physics by considering bosons and fermions in the same footing. This idea has the potential of solving many problems beyond standard model and in order to that it brought a new kind of symmetry into the picture. This new symmetry allows one to interchange between two seemingly very different kind of particles, bosons and fermions and it brings a new conserved quantity with it namely supercharge. The simplest case of SUSY quantum mechanics is 1D SUSY harmonic oscillator. There exists two parallel formalisms [5][3] for this system in the literature and both of them solve the problem uniquely. In this article we will discuss about how both of these formalisms are deeply related and will point out the equivalence of these two formalisms. At last we will also provide a Mathematica code to calculate and plot the eigenfunction of 1D supersymmetric partner Hamiltonian and present three examples of 1-D harmonic oscillator, 1-D infinite potential well and 1-d inverted harmonic oscillator with an anharmonic term αx^6.

[†]rathin.phy@iitb.ac.in
[‡]archana_phy@iitb.ac.in

[1]SUSY, supersymmetry; 1-D, 1 Dimensional; HO, Harmonic Oscillator; AHO, Anharmonic Oscillator; inf. pot., infinite potential

2. A BRIEF REVIEW OF TWO FORMALISMS FOR SUSY HARMONIC OSCILLATOR

Bosonic and fermionic harmonic oscillators are main building block of many physical theories. However, there is a mojor difference between the behaviour of these two particles[2]. By definition, bosons have integeral spin and fermions have half integeral spin. Moreover, according to Pauli exclusion principle no two identical fermions can occupy the same state but there is no such constraint for bosons. Also, we know that under the exchange of two identical fermions the wave function describing the state of these two particles takes up a minus sign but if we exchange two bosons no such minus sign appears in the wave function.
Now, to bring the bosonic and fermionic particles in the same footing 'supersymmetry' plays a crucial role and to incorporate them in a single frame one needs to build a common Hilbert space for both of them. There are mainly two ways of constructing the Hilbert space of this system that yield two different formalisms.

2.1 *Tensor product formalism*

The bosonic harmonic oscillator resides in a Hilbert space,$\mathcal{H}_{\mathcal{B}}$ that is $L^2(\mathcal{R})$ in nature and the Hilbert space of fermionic harmonic oscillator,$\mathcal{H}_{\mathcal{F}}$ is a $\mathcal{C}^2$ space. The ladder operators of bosonic harmonic oscillator are defined by their commutator relations and the ladder operator of fermionic harmonic oscillator are defined by their anti-commutator relation. Now one of the ways to construct the Hilbert space of SUSY harmonic oscillator is by going to a tensor product space of these two systems as

$$\mathcal{H}_{\mathcal{S}} = \mathcal{H}_{\mathcal{B}} \otimes \mathcal{H}_{\mathcal{F}}. \tag{1}$$

The basis of this Hilbert space is defined as

$$|n\rangle_S = |n\rangle_B \otimes |n\rangle_F,$$

where $|n\rangle_B$ and $|n\rangle_F$ are the number state basis of bosonic and fermionic harmonic oscillators respectively. An operator in this Hilbert space is defined as

$$\mathcal{O}_1 \otimes \mathcal{O}_2 : \mathcal{H}_{\mathcal{B}} \otimes \mathcal{H}_{\mathcal{F}} \rightarrow \mathcal{H}_{\mathcal{B}} \otimes \mathcal{H}_{\mathcal{F}}. \tag{2}$$

The Hamiltonian of the bosonic harmonic oscillator can be written as

$$H_B = \hbar\omega_B \left(a^\dagger a + \frac{1}{2}\right), \tag{3}$$

where $a^\dagger$ and a are respectively annihilation and creation operators defined as

$$a^\dagger = \frac{1}{\sqrt{2m\hbar\omega_B}} \left(-ip + m\omega_B x\right) \tag{4}$$

$$a = \frac{1}{\sqrt{2m\hbar\omega_B}} \left(ip + m\omega_B x\right). \tag{5}$$

The commutation relation between them is given by

$$\left[a, a^\dagger\right] = 1, [a, a] = 0, \quad \left[a^\dagger,\ a^\dagger\right] = 0, \tag{6}$$

and $N_B = a^\dagger a$ is the bosonic number operator. This operator acting on the n-th number state gives the number of bosonic particles of that particular state as the eigenvalue.

$$N_B|n\rangle_B = n_B|n\rangle_B, \qquad n_B = 0, 1, 2, .. \tag{7}$$

The energy eigenvalue equation for the above state can be written as

$$H_B|n\rangle_B = E_{n_B}|n\rangle_B = \left(n_B + \frac{1}{2}\right)\hbar\omega|n\rangle_B. \tag{8}$$

The operation of the creation and annihilation operators on the number states is given by

$$a^\dagger|n\rangle_B = \sqrt{n_B + 1}|n+1\rangle_B \tag{9}$$

$$a|n\rangle_B = \sqrt{n_B}|n-1\rangle_B. \tag{10}$$

On the other hand the Hamiltonian of fermionic harmonic oscillator is given by

$$H_F = \hbar\omega_F\left(c^\dagger c - \frac{1}{2}\right), \tag{11}$$

where c and $c^\dagger$ are respectively the fermionic annihilation and creation operator that satisfy the anti-commutation relation as

$$\{c, c^\dagger\} = 1, \quad \{c^\dagger, c^\dagger\} = 0, \quad \{c, c\} = 0. \tag{12}$$

The fermionic number operator is similarly defined as

$$N_F = c^\dagger c, \tag{13}$$

which acts on the n-th fermionic number state as

$$N_F|n\rangle_F = n_F|n\rangle_F, \qquad n_F = 0, 1. \tag{14}$$

The energy eigen value equation for this state would be written as

$$H_F|n\rangle_F = E_{n_F}|n\rangle_F = \left(n_F - \frac{1}{2}\right)\hbar\omega|n\rangle_F. \tag{15}$$

One property of fermionic creation and annihilation operators is that due to their anti-commutation relations, they are nilpotent of order 2 which means

$$\{c^\dagger, c^\dagger\}|n\rangle_F = 0 \tag{16}$$

$$\left(c^\dagger c^\dagger + c^\dagger c^\dagger\right)|n\rangle_F = 0$$

$$c^\dagger c^\dagger|n\rangle_F = -c^\dagger c^\dagger|n\rangle_F$$

$$c^\dagger c^\dagger|n\rangle_F = 0. \tag{17}$$

Similarly for the annihilation operator

$$cc|n\rangle_F = 0, \tag{18}$$

which only leaves two possible state in the fermionic ladder namely $|0\rangle$ and $|1\rangle$ that satisfies

$$c|0\rangle = 0 \ \ \& \ \ c^\dagger|1\rangle = 0. \tag{19}$$

Now we construct the Hilbert space of the joint system as of Eq.1 and keeping in mind the form of the operators in this Hilbert space as of Eq.2 we write the Hamiltonian of the Hilbert space of SUSY harmonic oscillator as

$$H_S = H_B \otimes \mathcal{I}_\mathcal{F} \ + \mathcal{I}_\mathcal{B} \otimes H_B \tag{20}$$

$$= \hbar\omega_B \left(a^\dagger a + \frac{1}{2}\right) \otimes \mathcal{I}_\mathcal{F} \ + \ \mathcal{I}_\mathcal{B} \otimes \left(c^\dagger c - \frac{1}{2}\right) \hbar\omega_F, \tag{21}$$

where $\mathcal{I}_\mathcal{B}$ and $\mathcal{I}_\mathcal{F}$ are the identities of bosonic and fermionic Hilbert spaces respectively. By using the number operator of respective spaces the energy eigenspectrum of the Hilbert space of SUSY harmonic oscillator becomes

$$E = E_B + E_F = \left(n_B + \frac{1}{2}\right) \hbar\omega_B \ + \ \left(n_F - \frac{1}{2}\right) \hbar\omega_F. \tag{22}$$

Likewise, We can define the number operator of this SUSY harmonic oscillator as

$$N_S = N_B \otimes \mathcal{I}_F \ + \ \mathcal{I}_B \otimes N_F. \tag{23}$$

We now come to the main part of the supersymmetry and define an operator Q called Supercharge and its conjugate $Q^\dagger$ as

$$Q = a \otimes c^\dagger \qquad \text{and} \qquad Q^\dagger = a^\dagger \otimes c. \tag{24}$$

These two operators acting on the number state of the Hilbert Space $\mathcal{H}_\mathcal{S}$ yield

$$Q^\dagger|n\rangle_S = \left(a^\dagger \otimes c\right)|n\rangle_B \otimes |n\rangle_F = |n+1\rangle_B \otimes |n-1\rangle_F \tag{25}$$

$$Q|n\rangle_S = \left(a \otimes c^\dagger\right)|n\rangle_B \otimes |n\rangle_F = |n-1\rangle_B \otimes |n+1\rangle_F. \tag{26}$$

These operators change one fermion to one boson and vice versa. So these two operators are called the generators of the supersymmetry. Now in Eq.1 if we take a simplifying assumption that $\omega_B = \omega_F = \omega$, H_S takes the form

$$H_S = \hbar\omega \left(\left(a^\dagger a + \frac{1}{2}\right) \otimes \mathcal{I}_\mathcal{F} \ + \ \mathcal{I}_\mathcal{B} \otimes \left(c^\dagger c - \frac{1}{2}\right)\right)$$

$$H_S = \hbar\omega \left(a^\dagger a \otimes \mathcal{I}_\mathcal{F} \ + \ \mathcal{I}_\mathcal{B} \otimes c^\dagger c\right). \tag{27}$$

Now it can be very easily shown that $Q^\dagger$ and Q commutes with H_S i.e.

$$[H_S, Q] = \left[H_S, Q^\dagger\right] = 0. \tag{28}$$

This implies that the system posses symmetry under the exchange of bosons and fermions and the supercharge is also a conserved quantity. Q and $Q^\dagger$ also obey the following anti-commutator relations

$$\{Q, Q^\dagger\} = H_S, \;\; \{Q, Q\} = 0 \;\text{ and }\; \{Q^\dagger, Q^\dagger\} = 0. \tag{29}$$

2.2 *Super-Potential Formalism*

This is a more general formalism and can handle various 1D SUSY systems unlike the tensor product formalism. Here the trick is also to factorise the Hamiltonian. We begin with 1D time independent Schrodinger's equation of the system of our interest as

$$H_1\psi_1^{(n)} = \left(-\frac{\hbar^2}{2m}\frac{d^2}{dx^2} + V_1(x)\right)\psi_1^{(n)} = E_1^{(n)}\psi_1^{(n)} \tag{30}$$

where $E_1^{(n)}$ and $\psi_1^{(n)}$ are the nth eigenvalue and eigenfunction of H_1. Therefore, we can express the potential in terms of the ground state eigenfunction and eigenvalue as

$$V_1(x) = \frac{\hbar^2}{2m}\frac{1}{\psi_1^{(0)}(x)}\frac{d^2\psi_1^{(0)}}{dx^2} + E_1^{(0)} \tag{31}$$

Now by defining $H_1 - E_1^{(0)}$ as H_B we can write it as

$$H_1 - E_1^{(0)} = H_B \tag{32}$$

$$= -\frac{\hbar^2}{2m}\frac{d^2}{dx^2} + \frac{\hbar^2}{2m}\frac{1}{\psi_1^{(0)}(x)}\frac{d^2\psi_1^{(0)}}{dx^2} \tag{33}$$

$$= -\frac{\hbar^2}{2m}\frac{d^2}{dx^2} + V_B, \quad \text{where } V_B = \frac{\hbar^2}{2m}\frac{1}{\psi_1^{(0)}(x)}\frac{d^2\psi_1^{(0)}}{dx^2}. \tag{34}$$

At this point we introduce two operators A and $A^\dagger$ in the following manner

$$\begin{aligned} A^\dagger &= -\frac{\hbar}{\sqrt{2m}}\frac{d}{dx} + W(x) \\ A &= \frac{\hbar}{\sqrt{2m}}\frac{d}{dx} + W(x), \end{aligned} \tag{35}$$

where $W(x)$ is known as Superpotential. With a little algebra we get

$$A^\dagger A = -\frac{\hbar^2}{2m}\frac{d^2}{dx^2} - \frac{\hbar}{\sqrt{2m}}W'(x) + W^2(x). \tag{36}$$

We can therefore factorise the Hamiltonian H_B as

$$H_B = A^\dagger A, \tag{37}$$

with the identification

$$V_B = W^2(x) - \frac{\hbar}{\sqrt{2m}} W'(x) = V_1 - E_1^{(0)}. \tag{38}$$

We denote the eigenvalues and eigenfunction of H_B as $E_B^{(n)}$ and $\psi_B^{(n)}$ respectively. Note that $\psi_B^{(n)}$ and $\psi_1^{(n)}$ are same and the eigenvalues $E_B^{(n)}$ are different from $E_1^{(n)}$ by a constant shift of $E_1^{(0)}$. Now comes the SUSY part and we define what we call "Partner Hamiltonian" of H_B as

$$H_F = AA^\dagger. \tag{39}$$

Using definition of A and $A^\dagger$ from Eq.35 we can write this equation as

$$H_F = -\frac{\hbar^2}{2m}\frac{d^2}{dx^2} + V_F(x) \tag{40}$$

$$\text{where, } V_F(x) = W^2(x) + \frac{\hbar}{\sqrt{2m}} W'(x). \tag{41}$$

We can denote the nth eigenvalue and eigenfunction of H_F as $E_F^{(n)}$ and $\psi_F^{(n)}$. These states posses some beautiful relations which will be very useful later. Note that using Eq.37 and Eq.39 we get

$$H_B\{A^\dagger \psi_F^{(n)}(x)\} = A^\dagger H_F \psi_F^{(n)}(x) = E_F^{(n)}\{A^\dagger \psi_F^{(n)}(x)\} \tag{42}$$

$$H_F\{A\psi_B^{(n)}(x)\} = AH_B \psi_B^{(n)}(x) = E_B^{(n)}\{A\psi_B^{(n)}(x)\} \tag{43}$$

This shows that $A^\dagger \psi_F^{(n)}(x)$ is an eigenstate of H_B and $A\psi_B^{(n)}(x)$ is an eigenstate of H_F. So $A^\dagger$ and A are intertwining operators that link the eigenstates of the two partner Hamiltonians H_B and H_F. With little algebra it can be shown that

$$\psi_F^{(n)} = \left(E_B^{(n+1)}\right)^{-1/2} A\psi_B^{(n+1)} \tag{44}$$

$$\psi_B^{(n+1)} = \left(E_F^{(n)}\right)^{-1/2} A^\dagger \psi_F^{(n)} \tag{45}$$

$$E_F^{(n)} = E_B^{(n+1)} \tag{46}$$

Now in this formalism to show the supersymmetric invariance of the system we go to direct sum space of $\mathcal{H}_\mathcal{B}$ and $\mathcal{H}_\mathcal{F}$ where Hamiltonian H_B belongs to $\mathcal{H}_\mathcal{B}$ Hilbert space and Hamiltonian H_F belongs to $\mathcal{H}_\mathcal{F}$ Hilbert space. So, we define the new Hilbert space and the Hamiltonian as

$$\mathcal{H}_\mathcal{S} = \mathcal{H}_\mathcal{B} \oplus \mathcal{H}_\mathcal{F} \qquad \text{and} \tag{47}$$

$$H_S = \begin{pmatrix} H_B & 0 \\ 0 & H_F \end{pmatrix} \tag{48}$$

and the super charge operator and its conjugate as

$$Q = \begin{pmatrix} 0 & 0 \\ A & 0 \end{pmatrix} \text{ and } Q^\dagger = \begin{pmatrix} 0 & A^\dagger \\ 0 & 0 \end{pmatrix}. \tag{49}$$

Now it is easy to show that these operators follow the same commutation and anti-commutation rules as of Eq.28 and Eq.29. We can write the SUSY wave function as

$$\psi_S^{(n)} = \begin{pmatrix} \psi_B^{(n)} \\ \psi_F^{(n)} \end{pmatrix} \tag{50}$$

but note that this is not an eigenstate of H_S due to Eq.46. We shall have to take the state as

$$\psi_S^{(n)} = \begin{pmatrix} \psi_B^{(n)} \\ \psi_F^{(n-1)} \end{pmatrix} \tag{51}$$

to make it an eigenstate of H_S. Now at this point the two formalisms seem to be using different techniques to deal with the problem of SUSY harmonic oscillator. So, in the next section we would like to discuss and illustrate how they are related and how the partner eigenstates are related to the number state of tensor product formalism.

3. EQUIVALENCE OF TENSOR PRODUCT AND PARTNER HAMILTONIAN FORMALISM FOR 1-D SUSY HARMONIC OSCILLATOR

To understand the equivalence of these two formalisms we have to first understand what $\psi_F^{(n)}$ and $\psi_B^{(n)}$ means physically. A system is called fermionic when the total spin of the system is half integral and we note that in 1-D harmonic oscillator the number of bosons can range from 0 to any large value but the number of fermion can be either 0 or 1. From Eq.32 we see that for 1-D harmonic oscillator $\psi_B^{(n)}$ has energy eigenvalue

$$E_B^{(n)} = E_1^{(n)} - E_1^{(0)} = n\hbar\omega. \tag{52}$$

This directly implies that there are total n bosons and 0 fermions in this state which is equivalent to $|n\rangle \otimes |0\rangle$ state of tensor product formalism or the nth bosonic excitation state of SUSY Hamiltonian of tensor product space. The fermionic partner Hamiltonian state $\psi_F^{(n)}$ refers a state where we have n bosons and 1 fermion making the total spin half integral and hence it is equivalent to the $|n\rangle \otimes |1\rangle$ state of tensor product formalism. By this comparison we can see clear physical meaning of Eq.46. From Eq.52 and Eq.46 we get $E_F^{(n)} = (n+1)\hbar\omega$. Using this idea of equivalence we can find it to be trivial that $\psi_F^{(n)}$ is a state containing n+1 particles and therefore, its energy is same as the energy of $|n\rangle \otimes |1\rangle$ state. From Eq.44 and Eq.45 we can now understand the operation of A and $A^\dagger$ on the partner eigenstates more clearly that they respectively create a fermion by destroying a boson and vice versa. This property was not that clear from equation 35. The normalisation constant of Eq.44 and Eq.45 can be calculated very easily. To derive Eq.44, Let us assume that

$$\psi_F^{(n)} = c_1 A \psi_B^{(n+1)} \tag{53}$$

where c_1 is the normalisation constant then by taking inner products we get

$$1 = c_1^2 \langle \psi_B^{(n+1)} | A^\dagger A | \psi_B^{(n+1)} \rangle \tag{54}$$

$$= c_1^2 \langle \psi_B^{(n+1)} | H_B | \psi_B^{(n+1)} \rangle \tag{55}$$

$$= c_1^2 E_B^{(n+1)} \tag{56}$$

$$\text{or,} c_1 = \left(E_B^{(n+1)} \right)^{-1/2} \tag{57}$$

we can do this similarly for Eq.45. Now we present a schematic diagram for visualising the connections between these formalisms and their corresponding states and energies.

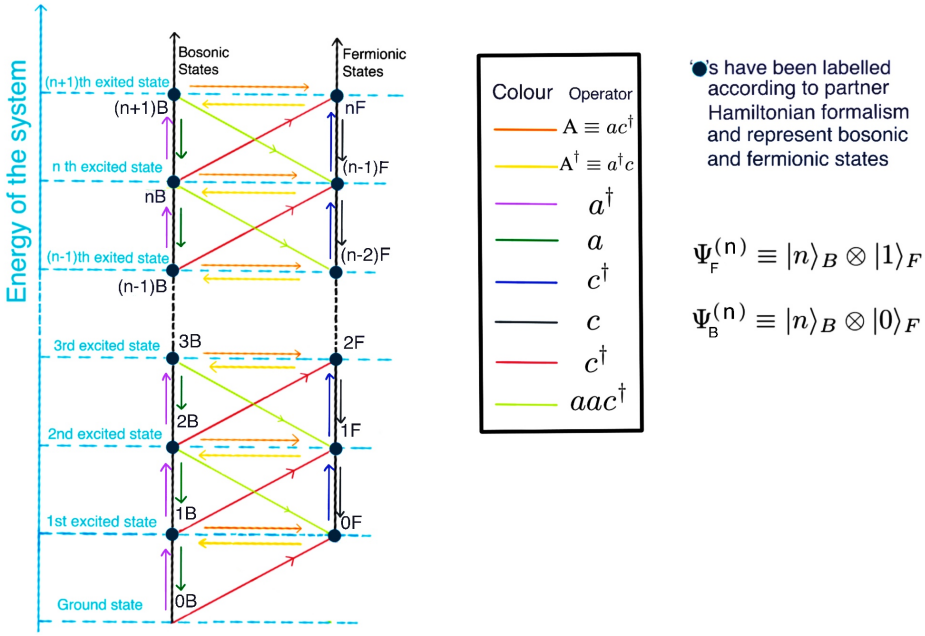

Figure 1. Schematic diagram of equivalence of tensor product and partner Hamiltonian formalism

In the partner Hamiltonian formalism the ground state is a bit special as there is no fermionic partner eigenstate for this and the ground state of SUSY harmonic oscillator is bosonic. In the diagram we have a pair of black vertical lines. The nodes on the left one of them represents the bosonic states whereas the nodes on the right one denotes the fermionic states and these states are

equidistant, marked by their corresponding level of excitation.
Here we give a table showing the equivalence of states of the two formalisms and their corresponding positions marked in the diagram. All the arrows represent the necessary operators for going from one state to another one.

Point in the diagram	Cor. TP state	Eqv. PH wave fn.	E of the state	n_B of the state	n_F of the state
0B	$\|0\rangle_B \otimes \|0\rangle_F$	$\psi_B^{(0)}$	0	0	0
0F	$\|0\rangle_B \otimes \|1\rangle_F$	$\psi_F^{(0)}$	$\hbar\omega$	0	1
1B	$\|1\rangle_B \otimes \|0\rangle_F$	$\psi_B^{(1)}$	$\hbar\omega$	1	0
1F	$\|1\rangle_B \otimes \|1\rangle_F$	$\psi_F^{(1)}$	$2\hbar\omega$	1	1
2B	$\|2\rangle_B \otimes \|0\rangle_F$	$\psi_B^{(2)}$	$2\hbar\omega$	2	0
2F	$\|2\rangle_B \otimes \|1\rangle_F$	$\psi_F^{(2)}$	$3\hbar\omega$	2	1
3B	$\|3\rangle_B \otimes \|0\rangle_F$	$\psi_B^{(3)}$	$3\hbar\omega$	3	0
(n-2) F	$\|n-2\rangle_B \otimes \|1\rangle_F$	$\psi_F^{(n-2)}$	$(n-1)\hbar\omega$	n-2	1
(n-1)B	$\|n-1\rangle_B \otimes \|0\rangle_F$	$\psi_B^{(n-1)}$	$(n-1)\hbar\omega$	n-1	0
(n-1) F	$\|n-1\rangle_B \otimes \|1\rangle_F$	$\psi_F^{(n-1)}$	$n\hbar\omega$	n-1	1
n B	$\|n\rangle_B \otimes \|0\rangle_F$	$\psi_B^{(n)}$	$n\hbar\omega$	n	0
n F	$\|n\rangle_B \otimes \|1\rangle_F$	$\psi_F^{(n)}$	$(n+1)\hbar\omega$	n	1
(n+1) B	$\|n+1\rangle_B \otimes \|0\rangle_F$	$\psi_B^{(n+1)}$	$(n+1)\hbar\omega$	n+1	0

Cor., Corresponding; TP, Tensor Product; Eqv., Equivalent; PH, Partner Hamiltonian;
fn, function; E, Energy; n_B, number of bosons; n_F, number of fermions;

Table 1. Table of equivalence

So we note that the index 'n' in partner Hamiltonian formalism irrespective of ψ_B or ψ_F represents the number of bosons in that state. Now as A destroys a boson and creates a fermion, for the bosonic ground state we can write

$$A\psi_B^{(0)}(x) = 0. \tag{58}$$

$$\text{This implies,} \quad W(x) = -\frac{\hbar}{\sqrt{2m}} \frac{1}{\psi_B^{(0)}} \frac{d\psi_B^{(0)}}{dx} \tag{59}$$

$$= -\frac{\hbar}{\sqrt{2m}} \frac{d\ln\left(\psi_B^{(0)}\right)}{dx}. \tag{60}$$

So, this equation completes the calculation of SUSY wave function for 1D cases as using equations 35, 44, 46, 60 we can calculate the partner wave functions of any 1-D SUSY quantum mechanical system as we show in the next section.

4. CALCULATION OF SUSY PARTNER WAVE FUNCTIONS FOR 1-D SUSY HARMONIC OSCILLATOR

In this section we calculate the eigenfunction of the fermionic Hamiltonian H_F. Now for 1-D harmonic oscillator we know that

$$H_1\psi_1^{(n)} = \left(-\frac{\hbar^2}{2m}\frac{d^2}{dx^2} + \frac{1}{2}m\omega^2x^2\right)\psi_1^{(n)} = E_1^{(1)}\psi_1^{(n)}. \tag{61}$$

The eigenfunction and and the energy eigenvalues are given by

$$\psi_1^{(n)} = \left(\frac{m\omega}{\pi\hbar}\right)^{1/4}\frac{1}{\sqrt{2^n n!}}\exp\left(-\frac{m\omega}{2\hbar}x^2\right)H_n\left[\left(\frac{m\omega}{\hbar}\right)^{1/2}x\right] \tag{62}$$

where, $H_n(x)$ are Hermite polynomials and

$$E_1^{(n)} = \left(n + \frac{1}{2}\right)\hbar\omega. \tag{63}$$

So, as we have discussed earlier that $\psi_1^{(n)} = \psi_B^{(n)}$ and $E_B^{(n)} = n\hbar\omega$. The ground state wave function of $\psi_B^{(n)}$ and its derivative is given by

$$\psi_B^{(0)} = \left(\frac{m\omega}{\pi\hbar}\right)^{1/4}\exp\left(-\frac{m\omega}{2\hbar}x^2\right) \text{ and } \frac{d}{dx}\psi_B^{(0)} = -x\frac{m\omega}{\hbar}\psi_B^{(0)}. \tag{64}$$

From Eq.60 we get

$$W(x) = \frac{\hbar}{\sqrt{2m}}\frac{m\omega}{\hbar}x = \sqrt{\frac{m}{2}}\omega x. \tag{65}$$

So, now from Eq.41 we can write

$$V_F(x) = \frac{m\omega^2}{2}x^2 + \frac{1}{2}\hbar\omega, \tag{66}$$

and from Eq.46 we get

$$E_F^{(n)} = (n+1)\hbar\omega. \tag{67}$$

Now, from Eq.44 and Eq.35 we can write the form of eigenstate of H_F as

$$\psi_F^{(n)} = \frac{1}{\sqrt{E_B^{(n+1)}}}A\psi_B^{(n+1)} \tag{68}$$

$$= \frac{1}{\sqrt{(n+1)\hbar\omega}}\left(\frac{\hbar}{\sqrt{2m}}\frac{d}{dx} + W(x)\right)\left(\mathcal{N}\exp\left(-\frac{m\omega x^2}{2\hbar}\right)H_n\left[\left(\frac{m\omega}{\hbar}\right)^{1/2}x\right]\right), \tag{69}$$

where $\mathcal{N}$ is the corresponding normalisation constant.

Now after doing the simplification we get

$$\psi_F^{(n)} = \left(\frac{m\omega}{\pi\hbar}\right)^{1/4} \frac{1}{\sqrt{2^n n!}} \exp\left(-\frac{m\omega}{2\hbar}x^2\right) H_n\left[\left(\frac{m\omega}{\hbar}\right)^{1/2} x\right]. \tag{70}$$

We see that the form of eigenfunctions are same for H_B and H_F in the case of 1-D SUSY harmonic oscillator which is a well known example of shape invariant potential [1] in supersymmetric quantum mechanics.

5. MATHEMATICA CODE

In this section we present a Mathematica code using which one can calculate the eigenfunctions of H_B and H_F for any 1-D SUSY quantum mechanical system. The plots of the eigenfunctions have been made in two different ways. Firstly, we have used the superpotential formalism in order to obtain $\psi_F^{(n)}$ from $\psi_B^{(n)}$ as shown in previous section. Secondly, we have used the analytical solution of the partner eigenfunction to plot it.The first method is a more general numerical way of obtaining the supersysmmetric partner eigenfunction even for the cases when it is hard to solve the schrodinger equation of the system analytically.
We can observe that the plot of the wavefunctions made in two different ways matches perfectly.

SUSY 1 - D Harmonic Oscillator

```
In[•]:= Clear["Global`*"];
```

■ Value of the Parameters : -

```
In[•]:= ħ = 1; m = 1/2; ω = 1;
```

■ Potential : -

```
In[•]:= V₁[x_] := 1/2 m ω^2 x^2;
```

■ Hamiltonian : -

```
In[•]:= H₁ = -ħ^2/(2 m) * u''[x] + V₁[x] * u[x];
```

■ Obtaining Eigenvalues and Eigenfunctions (Ground State to 5th Excited State) of 1 D Harmonic Oscillator : -

```
In[•]:= {Eigenvalue, Eigenfunction} = NDEigensystem[H₁, u[x], {x, -100, 100}, 6,
          Method →
           {"SpatialDiscretization" ->
             {"FiniteElement", {"MeshOptions" -> {"MaxCellMeasure" -> 0.01}}}}];
```

Out[•]=

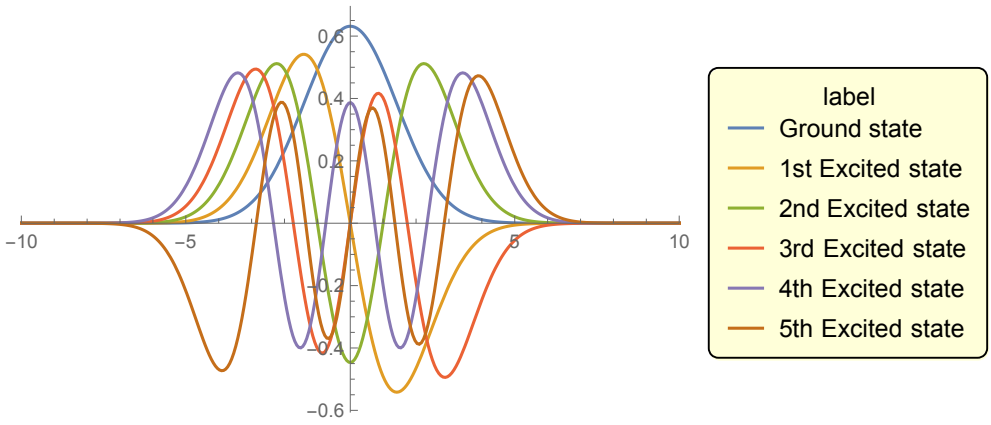

Figure 2. Numerical plots of the first 6 eigenstates of bosonic HO hamiltonian

■ Defining : -

```
In[•]:= E₁[n_] := Eigenvalue[[n]];
```

NOTE : Array indexing starts from 1 in Mathematica. So n = 1 is the Ground State in this case.

■ Energy Eigenvalue and Eigenfunction of Bosonic Hamiltonian H_B : –

```
In[•]:= E_B[n_] := E_1[n] - E_1[1];
        ψ_B[n_] := Eigenfunction[[n]];
```

■ Superpotential : -

```
In[•]:= W = -ψ_B[1]^(-1) * D[ψ_B[1], x];
```

■ Fermionic Eigenfunction or Eigenfunction of the Partner Hamiltonian (H_F) : –

$$\blacksquare\ \psi_F^{(n)} = \left(E_B^{(n+1)}\right)^{-\frac{1}{2}} \left(\frac{\hbar}{\sqrt{2m}}\frac{d}{dx} + W(x)\right) \psi_B^{(n+1)}$$

```
In[•]:= ψ_F[n_] := (E_B[n + 1])^(-1/2) * (ħ/√(2m)) D[ψ_B[n + 1], x] + W * ψ_B[n + 1]
```

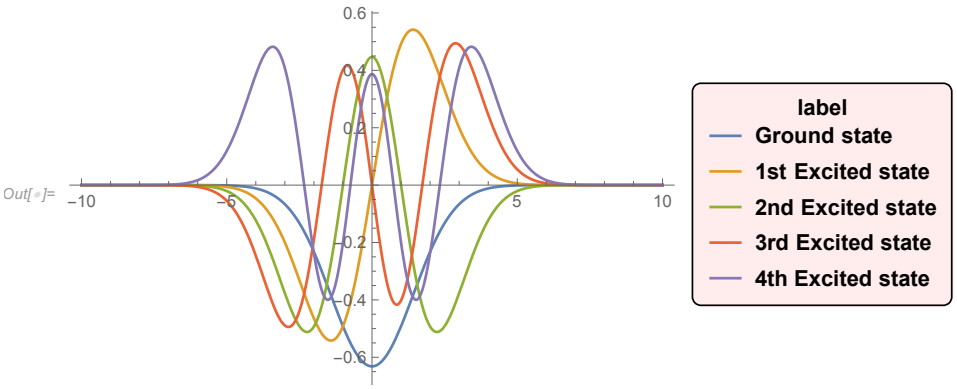

Figure 3. Numerical plots of the first 5 eigenstates of fermionic HO hamiltonian

The Analytic Solution of the Partner Hamiltonian Eigenfunction : -

■ Parameters : -

```
In[•]:= m = 1/2; ω = 1; ħ = 1;
```

Now by using the form of Eq. 70 we define,

```
In[•]:= ϕF[n_, x_] := (m*ω/π)^(1/4) 1/√(2^n n!) Exp[-(m*ω)/(2 ħ) x^2] HermiteH[n, (m*ω/ħ)^(1/2) x]
```

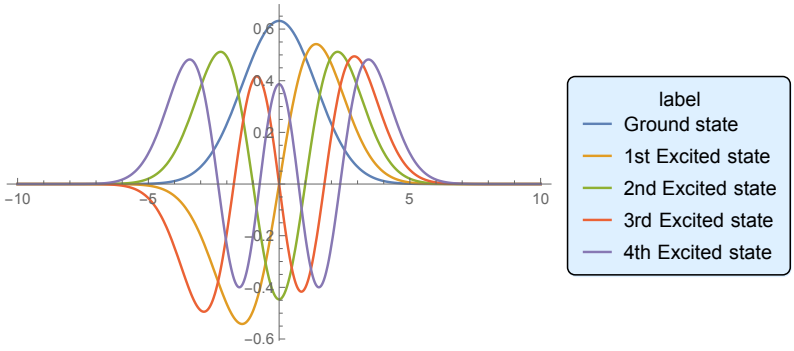

Figure 4. Plots of the first 5 analytical solutions of HO eigenstates

NB : The plots of ψ_F and ϕ_F are same apart from a random sign flip. This sign is actually inherited from the method that Mathematica uses for solving the differential equations. However it doesn't matter because if ψ_F is an eigenfunction of H_F then $(-\psi_F)$ is also an eigenfunction of H_F with the same eigenvalue.

Changing the value of the potential $V_1(x)$ we can plot the partner eigenfunction for any 1D SUSY Quantum System. Below we are showing the same thing for an 1D Infinite Potential Box. For the analytic solution we have considered the form of the partner eigenfunction as given in [4].

SUSY 1 D InfinitePotential Box

■ Values of the Parameters : -

```
In[•]:= ħ = 1; m = 1/2;
```

■ Potential : -

```
In[•]:= V1[x_] := 0;
```

■ Hamiltonian : -

```
In[•]:= H1 = -ħ^2/(2 m) * u''[x] + V1[x] * u[x];
```

■ Boundary Condition : -

```
In[•]:= B = DirichletCondition[u[x] == 0, True];
```

■ Obtaining Eigenvalues and Eigenfunctions(Ground State to 5th Excited State) of 1D Infinite Potential Box :-

```
In[•]:= {Eigenvalue, Eigenfunction} = NDEigensystem[{H1, B}, u[x], {x, 0, 1}, 6,
          Method → {"Eigensystem" → {"Arnoldi",
              "MaxIterations" → 10000},
            "PDEDiscretization" → {"FiniteElement", "MeshOptions" → {"MaxCellMeasure" → 0.001}}}];
```

Out[•]=

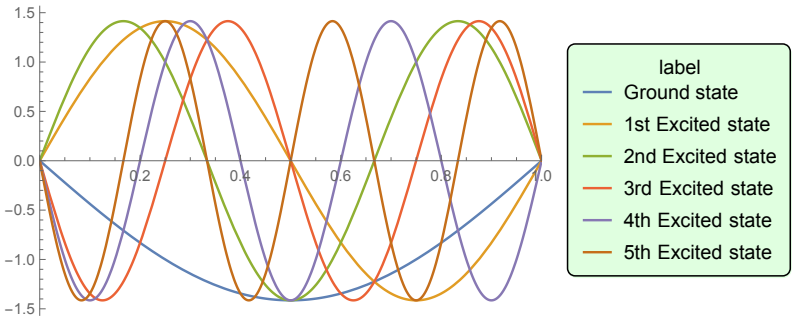

Figure 5. Numerical plots of the first 6 eigenstates of bosonic HO hamiltonian

Defining:-

```
In[•]:= E₁[n_] := Eigenvalue[[n]];
```

■ Energy Eigenvalue and Eigenfunction of Bosonic Hamiltonian H_B : –

```
In[•]:= E_B[n_] := E₁[n] - E₁[1];
        ψ_B[n_] := Eigenfunction[[n]];
```

■ Superpotential : -

```
In[•]:= W = -ψ_B[1]^(-1) * D[ψ_B[1], x];
```

■ Fermionic Eigenfunction or Eigenfunction of the Partner Hamiltonian (H_F) : –

$$\blacksquare\ \psi_F^{(n)} = \left(E_B^{(n+1)}\right)^{-\frac{1}{2}} \left(\frac{\hbar}{\sqrt{2m}}\frac{d}{dx} + W(x)\right) \psi_B^{(n+1)}$$

```
In[•]:= ψ_F[n_] := (E_B[n + 1])^(-1/2) * (ħ/√(2 m)) D[ψ_B[n + 1], x] + W * ψ_B[n + 1]
```

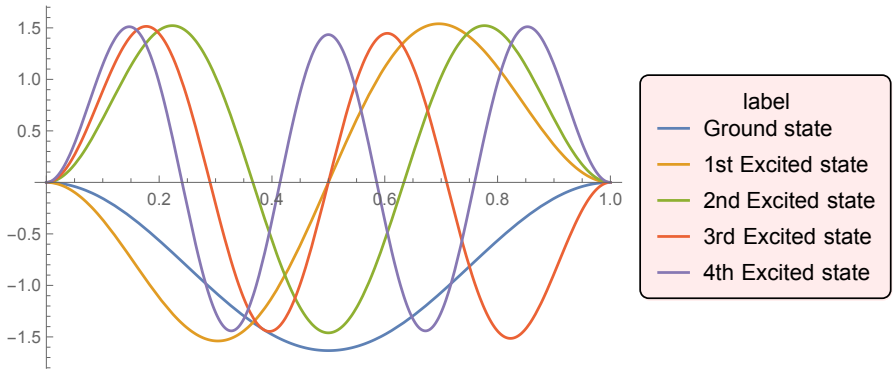

Figure 6. Numerical plots of the first 5 eigenstates of fermionic 1-D inf. pot. box hamiltonian

The Analytic Solution of the Partner Hamiltonian Eigenfunction : -

■ Parameter : -

```
In[•]:= L = 1;
```

```
In[•]:= ϕF[n_, x_] := √(2 / (L ((n + 2) ^2 - 1))) ((n + 2) * Cos[(n + 2) π/L x] - Cot [π/L x] * Sin [(n + 2) π/L x])
```

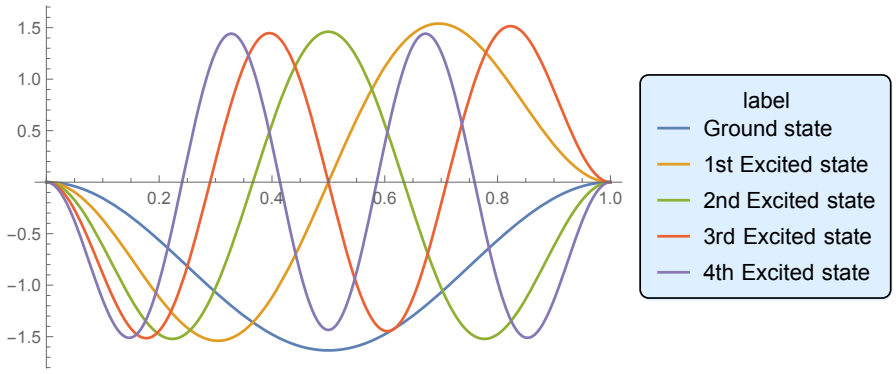

Figure 7. Plots of the first 5 analytical solutions of 1-D inf. pot. box hamiltonian eigenstates

Now we present the results for a case which can not be studied analytically without perturbation theory, the inverted harmonic oscillator. Here we have used the following form of potential;

$$V_1(x) = -\frac{1}{2}m\omega^2 x^2 + \alpha x^6 \tag{71}$$

Using this code we can very easily calculate its partner wave function numerically. We have here plotted only first few of them.

SUSY 1 - D Anharmonic Oscillator

■ Value of the Parameters : -

```
In[•]:= ħ = 1; m = 1/2; ω = 1; α = 1;
```

■ Potential : -

```
In[•]:= V1[x_] := -1/2 m ω^2 x^2 + α x^6;
```

■ Hamiltonian : -

```
In[•]:= H1 = -ħ^2/(2 m) * u''[x] + V1[x] * u[x];
```

■ Obtaining Eigenvalues and Eigenfunctions (Ground State to 3rd Excited State) of 1D Harmonic Oscillator : -

```
In[•]:= {Eigenvalue, Eigenfunction} =
          NDEigensystem[H1, u[x], {x, -100, 100}, 4,
           Method →
            {"SpatialDiscretization" ->
              {"FiniteElement", {"MeshOptions" -> {"MaxCellMeasure" -> 0.01}}}}];
```

Out[•]=

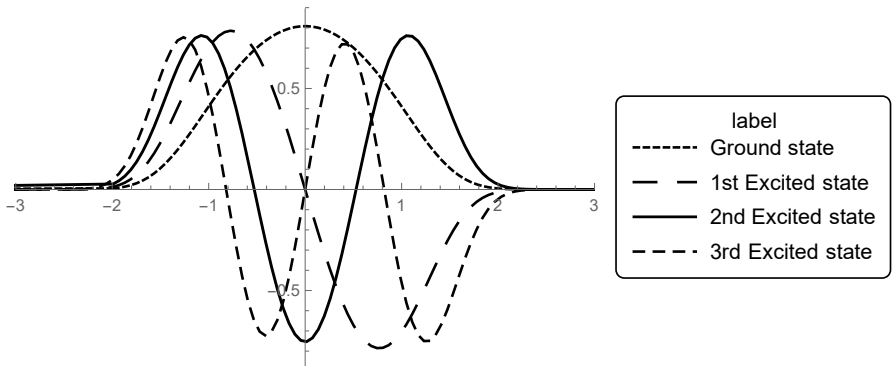

Figure 8. Numerical plots of the first 4 eigenstates of bosonic AHO hamiltonian

■ Defining : -

```
In[•]:= E1[n_] := Eigenvalue[[n]];
```

NOTE : Array indexing starts from 1 in Mathematica. So n = 1 is the Ground State in this case.

■ Energy Eigenvalue and Eigenfunction of Bosonic Hamiltonian H_B : –

```
In[•]:= E_B[n_] := E_1[n] - E_1[1];
        ψ_B[n_] := Eigenfunction[[n]];
```

■ Superpotential : -

```
In[•]:= W = -ψ_B[1]^(-1) * D[ψ_B[1], x];
```

■ Fermionic Eigenfunction or Eigenfunction of the Partner Hamiltonian (H_F) : –

■ $\psi_F^{(n)} = \left(E_B^{(n+1)}\right)^{-\frac{1}{2}} \left(\frac{\hbar}{\sqrt{2m}}\frac{d}{dx} + W(x)\right) \psi_B^{(n+1)}$

```
In[•]:= ψ_F[n_] := (E_B[n + 1])^(-1/2) * (ħ/√(2 m)) D[ψ_B[n + 1], x] + W * ψ_B[n + 1]
```

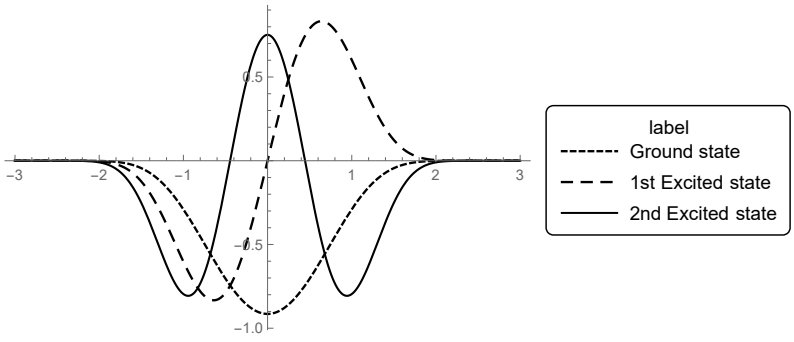

Figure 9. Numerical plots of the first 3 eigenstates of fermionic AHO hamiltonian

6. CALCULATION OF POTENTIAL FROM A SUITABLE GROUND STATE

Now we deal with a different problem where we first take a suitable ground state wave function and then try to find out what form of potential would be needed to generate this ground state wave function and moreover, we can also solve the Schrodinger's equation for that potential to find out higher excited eigenstates and their corresponding eigenvalues. So for that purpose we take the ground eigenstate of the form,

$$\psi = Ae^{-Bx^4} \tag{72}$$

and normalize it. By normalising we get,

$$\psi = \left[\frac{(2B)^{\frac{1}{4}}}{2\Gamma\left(\frac{5}{4}\right)}\right]^{\frac{1}{2}} e^{-Bx^4} \tag{73}$$

where $\Gamma(n)$ is the well known Gamma function. Now we can calculate W using Eq.60 as,

$$W = -\frac{1}{\sqrt{2}}\frac{d}{dx}(\ln\psi) = \frac{4}{\sqrt{2}}Bx^3 \tag{74}$$

where we have considered $\hbar = m = 1$. Then using Eq.38 and Eq.41, we can obtain V_B and V_F as,

$$V_B = W^2 - \frac{1}{\sqrt{2}}W' = 8B^2x^6 - 6Bx^2 \tag{75}$$

$$V_F = W^2 + \frac{1}{\sqrt{2}}W' = 8B^2x^6 + 6Bx^2 \tag{76}$$

Now to get a standard form and to proceed with the numerical calculations, we choose B=$\frac{1}{12}$ and we write V_B and V_F as,

$$V_B = \frac{1}{18}x^6 - \frac{1}{2}x^2 \tag{77}$$

$$V_F = \frac{1}{18}x^6 + \frac{1}{2}x^2 \tag{78}$$

This potential can be substituted in the Mathematica code presented in the previous section to get the energy eigenvalues and the higher energy eigenstates. Analytical and numerical solutions of Schrodinger's equation for similar kind of potential have been studied by several authors [6–9]. They have considered the general problem with the potential $ax^6 - bx^2$ and have calculated the exact analytical or numerical solutions for specific values of a and b.

7. CONCLUSION

In this paper we have discussed the equivalence of partner Hamiltonian and tensor product formalism which is an important idea to understand the framework of SUSY 1-D quantum mechanical systems. The Mathematica code can be used to get the partner eigenstates for very general 1-D potentials also for which we can get perturbative analytic solutions only as we have shown in the example of inverted harmonic oscillator with anharmonic term .

References

[1] Bagchi, B.K. *"Supersymmetry in quantum and classical mechanics",*(2001).

[2] Naber, Gregory *"Foundations of Quantum Mechanics:An Introduction to the Physical Background and Mathematical Structure",*(2015).

[3] Cooper, F., Khare, A., Sukhatme, U.(1995). *"Supersymmetry and quantum mechanics", Phys. Rep.* **251**, *267-385*.

[4] Kulkarni, A., Ramadevi, P.(2003). *"Supersymmetry", Reson* **8**, *28-41*, doi: 10.1007/BF02835648

[5] T. Wellman, *"An introduction to supersymmetry in quantum mechanical systems", Brown University Memorandum*,(2003).

[6] S. Brajamani & P. S. Mazumdar, *"Quantum normal form and the harmonic oscillator with x^6 perturbation",* (April 1988), *International Journal of Theoretical Physics* **27**, 397399.

[7] Dai-Nam Le, Ngoc-Tram D. Hoang, Van-Hoang Le *"Exact analytical solutions of the Schrdinger equation for a two dimensional purely sextic double-well potential"*, (March 2018), *Journal of Mathematical Physics* **59**, doi: 10.1063/1.4997532.

[8] Boya, Luis J. and Kmiecik, Michael and Bohm, A., *"Calculations with supersymmetric potentials"*, *Phys. Rev. D* **35**, 1255, doi: 10.1103/PhysRevD.35.1255

[9] P Roy et al, (1988), *"Remarks on negative energy states in supersymmetric quantum mechanics"*, *J. Phys. A: Math. Gen.* **21** 3673, doi: 10.1088/0305-4470/21/18/019.

Demonstration of a Quantum Harmonic Oscillator by involving Higher Qubit States and further associating it to a Bosonic System

Rajdeep Tah[1]*, **Bikash K. Behera**[2] **and Prasanta K. Panigrahi**[2†]
[1]3rd Semester (2nd Year), Integrated MSc., School of Physical Sciences
[1]National Institute of Science Education and Research, Bhubaneswar, HBNI, P.O. Jatni, Khurda-752050, Odisha, India.
[2]Department of Physical Sciences
[2]Indian Institute of Science Education and Research Kolkata, Mohanpur- 741246, West Bengal, India

Abstract. Here, we simulate a discretized quantum oscillator on a digital quantum computer provided by the IBM quantum experience platform. The simulation is carried out in two spatial dimensions and directions are provided for its extension to n-spatial dimensions. Further, we outline the necessary formulations for relevant operators and using them, we perform simulation of a particle in a discretized quantum harmonic oscillator potential using higher qubit system especially a five-qubit system. Finally we attempt to link the QHO (Quantum Harmonic Oscillator) to a Bosonic system and study it. We associated the concept of Pauli Matrix equivalent to Bosonic Particles and used it to calculate the Unitary Operators which helped us to theoretically visualize each Quantum states and further simulate our system.

Keywords. Quantum Harmonic Oscillator, Pauli Matrix equivalents, Bosonic System, Quantum States, Rabi Hamiltonian, Creation and Annihilation Operators, Unitary operator.

1. INTRODUCTION

Harmonic oscillator is one of the most fundamental problems in the field of Physics and it is involved in all aspects of Physics. The reason is still unknown to us but it is very natural for us to understand that whenever a system is disturbed from its minimum energy state then in the course of attaining minimum energy state again, the system will tend to oscillate. This is how a harmonic oscillator functions in a classical sense. Hence, it is worth to search for such a system in the quantum world, too. Thus, Quantum Harmonic Oscillator is nothing but a quantum mechanical analog of the classical harmonic oscillator.

A Quantum Harmonic Oscillator is different from a Classical Harmonic Oscillator mainly on the basis of three grounds: First, the ground energy state for a quantum harmonic oscillator is non-zero because there exists fluctuations as a result of Heisenberg Uncertainty Principle: Second, a particle in a quantum harmonic oscillator potential can be found outside the region -A $\leq x \leq$ +A with a non-zero probability: Thirdly, the probability density distributions for a quantum oscillator in the

*rajdeep.tah@niser.ac.in
†pprasanta@iiserkol.ac.in

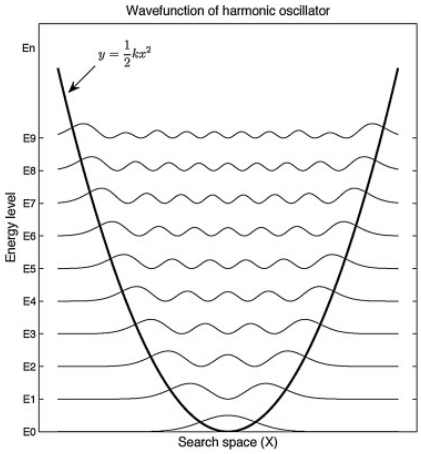

Figure 1. A Generalized Representation of Quantum Harmonic Oscillator

ground low-energy state is largest at the middle of the well. It is commonly used as a model to study the vibrations of the atomic particles and molecules under the effect of classical spring like potential which is a commonly accepted model for the molecular bonding. QHO (quantum harmonic oscillator) is one of the exactly solvable models in the field of quantum mechanics having solutions in the form of Hermite polynomials and it can be generalized to N-dimensions. Its application is not only restricted to the study of simple di-atomic molecule, but it's in fact expanded to the different domains of Physics, e.g. in the study of complex modes of vibration in larger molecule, the theory of heat capacity, QHO as a thermodynamic heat engine, etc.

2. HARMONIC OSCILLATOR IN BRIEF

The most common and familiar version of the Hamiltonian of the Quantum Harmonic Oscillator in general can be written as:

$$\hat{H} = \frac{\hat{p}^2}{2m} + \frac{1}{2}m\omega^2\hat{x}^2 = \frac{\hat{p}^2}{2m} + \frac{1}{2}k\hat{x}^2 \tag{1}$$

Where $\hat{H}$ is the Hamiltonian of the System, m is the mass of the particle, k is the bond stiffness (which is analogous to spring constant in classical mechanics), $\hat{x}$ is the position operator and $\hat{p} = -i\hbar\frac{\partial}{\partial x}$ is the momentum operator (where $\hbar$ is the reduced Plank's constant).
The analytical solution of the Schrodinger wave equation is given by[1]:

$$\Psi = \sum_{n_x=0}^{\infty}\sum_{n_y=0}^{\infty}\frac{1}{2^n\, n!}\left(\frac{m\omega}{\pi\hbar}\right)^{1/2} e^{-\frac{\zeta^2}{2}} e^{-\frac{\beta^2}{2}} H_{n_x}(\zeta)H_{n_y}(\beta)U(t) \tag{2}$$

Where;

$$\zeta = \sqrt{\frac{m\omega}{\hbar}}x \quad \text{and} \quad \beta = \sqrt{\frac{m\omega}{\hbar}}y$$

Here H_n is the nth order Hermite polynomial. U(t) is the Unitary Operator of the system showing its time evolution and is given by:

$$U(t) = exp\left(\frac{-itE_n}{\hbar}\right) = e^{\frac{-itE_n}{\hbar}} \tag{3}$$

Where E_n are the allowed energy eigenvalues of the particle and are given by:

$$E_n = (n_x + \frac{1}{2})\hbar\omega + (n_y + \frac{1}{2})\hbar\omega = (n_x + n_y + 1)\hbar\omega \tag{4}$$

And the states corresponding to the various energy eigenvalues are orthogonal to each other and satisfy:

$$\int_{-\infty}^{+\infty} \psi_j \psi_x dx_i = 0 : \forall\, x_i \tag{5}$$

A much simpler approach to the harmonic oscillator problem lies in the use of ladder operator method where we make use of ladder operators i.e. the creation and annihilation operators $(\hat{b}^\dagger, \hat{b})$, to find the solution of the problem.
Here $\hat{b}^\dagger$ denotes the 'Creation' operator and $\hat{b}$ denotes the 'Annihilation' operator in Bosonic System. We can also the Hamiltonian in terms of the creation and annihilation operators $(\hat{b}^\dagger, \hat{b})$[2]:

$$\hat{H} = \hbar\omega(\hat{b}\hat{b}^\dagger - \frac{1}{2}) = \hbar\omega(\hat{b}\hat{b}^\dagger + \frac{1}{2})$$

Now the Hamiltonian for "a discrete quantum harmonic oscillator" is given by:

$$\hat{H} = \frac{(\hat{p}^d)^2}{2} + \frac{(\hat{x}^d)^2 + (\hat{y}^d)^2}{2} \tag{6}$$

Where $\hat{p}^d$ is the discrete momentum operator and $\hat{x}^d$ and $\hat{y}^d$ are the discrete position operators in in x and y spatial dimension respectively. Also $\hat{p}^d$ can be expressed as:

$$\hat{p}^d = (F^d)^{-1} \cdot \hat{x}^d \cdot (F^d) \tag{7}$$

Where F^d is the standard discrete Quantum Fourier Transform matrix[3].

3. DISCRETIZATION OF THE SPACE

Generally, Discretization is the process of transforming the continuous functions, models and so on into their discrete counterparts. In fact, it is a necessity because to perform any kind of calculation on

machines like quantum computers, one needs to work with specific number of elements so that one can obtain outputs which have valid meanings over realistic time scales. However, the Hamiltonian in Eq.(1) allows a continuous eigenspectrum of position. That is why, we have to discretize the space. The Hamiltonian for "a discrete quantum harmonic oscillator" is given by:

$$\hat{H} = \frac{(\hat{p}^d)^2}{2} + \frac{(\hat{x}^d)^2 + (\hat{y}^d)^2}{2} \tag{8}$$

Where $\hat{p}^d$ is the discrete momentum operator and $\hat{x}^d$ and $\hat{y}^d$ are the discrete position operators in x and y spatial dimension respectively. Now let us consider N number of finite elements in a two dimensional space where $x, y \in [-L, +L]$ such that a mesh of N^2 number of elements can be created with each mesh point corresponding to a particular eigenvalue of x and y (A list of 5-qubit states and their corresponding mesh points are given in the following table). Assuming the Harmonic Oscillator potential to be centred at (0,0), we can write the position operator in the form of $N \times N$ matrix with all the position eigenvalues lying along its diagonal as:

$$[\hat{x}^d] = \sqrt{\frac{2\pi}{N}} \begin{bmatrix} -N/2 & 0 & 0 & . & 0 \\ 0 & (-N/2)+1 & 0 & . & 0 \\ . & . & . & . & . \\ 0 & 0 & . & . & . \\ 0 & 0 & 0 & . & (N/2)-1 \end{bmatrix} \tag{9}$$

5-qubit state	Mesh point
$\|00000\rangle$	x_i = -16
$\|00001\rangle$	x_i = -15
$\|00010\rangle$	x_i = -14
.	. .
.	. .
$\|11111\rangle$	x_i = 15

TABLE I. 5-Qubit state vs Mesh Point

The momentum operator ($\hat{p}^d$) can also be calculated in the same way. But to ease our calculation in finding the momentum eigenvalue for each position eigenfunction, we try to make the quantum Fourier transform of the wave function. This helps us to transform the wave function to momentum space where the momentum operators apply multiplicatively and the momentum eigenvalues will be the same as the position eigenvalues for respective discretized space points. An inverse discrete quantum Fourier transform can then be performed to bring back the function into Cartesian-space. The discrete momentum operator can then be applied as a $N \times N$ matrix given by:

$$\hat{p}^d = (\hat{F}^d)^{-1} \cdot \hat{x}^d \cdot (\hat{F}^d) \tag{10}$$

Where $\hat{F}^d$ is the standard discrete Quantum Fourier Transform matrix[3]. Each element of $\hat{F}^d$ can be expressed as:

$$[\hat{F}^d]_{j,k} = \frac{exp(2i\pi jk/N)}{\sqrt{N}} \tag{11}$$

Where $j, k \in [-\frac{N}{2}, ..., \frac{N}{2} - 1]$ and j= no. of rows in the matrix and k= no. of columns in the matrix.
This process is applicable for larger systems and we can have both position and momentum operator. We can also compute the unitary operator for studying the evolution of our system over time.

4. UNITARY TRANSFORMATION

For the sake of reducing mathematical complexity, let us assume $\hbar$, ω and m is unity (i.e. all are having value 1). So, we can write the Schrodinger equation as:

$$i\frac{\partial \Psi}{\partial t} = \hat{H}\Psi \tag{12}$$

Which further implies:

$$\Psi(t) = \Psi(0)exp(-i\hat{H}t) \tag{13}$$

From the above, it is vivid that the Unitary Operator to be computed is $U(t) = exp(-i\hat{H}^d t)$ where; $\hat{H}^d$ is the Discretized Hamiltonian Operator mentioned in Eq.(8). So, the Unitary Operator is given by:

$$U(t) = exp\bigg(- it\bigg(\frac{(\hat{p}^d)^2}{2} + \frac{(\hat{x}^d)^2 + (\hat{y}^d)^2}{2} \bigg) \bigg)$$

Or if we consider the X-dimension only, then we get the Unitary Operator as:

$$U_{\hat{x}}(t) = exp\bigg(\frac{-it}{2}((F^d)^{-1} \cdot \hat{(}x^d)^2 \cdot (F^d) + (\hat{x}^d)^2) \bigg) \tag{14}$$

Due to the discretization of space; the position operator $[\hat{x}^d]$, being a diagonal matrix, can be expanded by using the concept of Matrix exponential as Ref.[4]:

$$exp\bigg(- \frac{it}{2}[A] \bigg) = \mathbb{I} + \sum_{m=1}^{\infty} \bigg(- \frac{it}{2} \bigg)^m \frac{[A]^m}{m!} \tag{15}$$

Here A is the corresponding Operator Matrix and by using the matrix in this form, a time evolution can be performed for any arbitrary state. Such an evolution can be carried out using n-qubits in a quantum circuit.

5. QUANTUM SIMULATION

In our simulation we make use of 5 qubits for our simulation, so we consider 2^5 dimensional Hilbert space (since for a n-qubit system $N = 2^n$). Each dimension in the Hilbert space corresponds to an eigenfunction of a particular position eigenvalue. For two spatial dimensions; $x, y \in [-16, 16]$ and our space is discretized into $32 \times 32 = 1024$ individual mesh points. In order to construct quantum gates, we need to compute the unitary operator matrix. From Equation (4), the position operator in its matrix form can be written as:

$$[\hat{x}^d] = \sqrt{\frac{\pi}{16}} \begin{bmatrix} -16 & 0 & 0 & 0 & . & . & . & 0 \\ 0 & -15 & 0 & 0 & . & . & . & 0 \\ 0 & 0 & -14 & 0 & . & . & . & 0 \\ 0 & 0 & 0 & -13 & . & . & . & 0 \\ . & . & . & . & . & . & . & . \\ 0 & 0 & 0 & 0 & . & . & 14 & 0 \\ 0 & 0 & 0 & 0 & . & . & 0 & 15 \end{bmatrix} \tag{16}$$

Previously we have seen that $[\hat{x}^d]$ does not hold the sole importance. Because of the structure of the Hamiltonian, $[\hat{x}^d]^2$ plays a huge role for computing unitary operators for kinetic and potential energy portion individually. We can clearly see that $[\hat{x}^d]^2$ is a diagonal matrix with each diagonal element equal to corresponding position eigenvalue squared and is given by:

$$[\hat{x}^d]' = [\hat{x}^d]^2 = \frac{\pi}{16} \begin{bmatrix} 256 & 0 & 0 & 0 & . & . & . & 0 \\ 0 & 225 & 0 & 0 & . & . & . & 0 \\ 0 & 0 & 196 & 0 & . & . & . & 0 \\ 0 & 0 & 0 & 169 & . & . & . & 0 \\ . & . & . & . & . & . & . & . \\ 0 & 0 & 0 & 0 & . & . & 196 & 0 \\ 0 & 0 & 0 & 0 & . & . & 0 & 225 \end{bmatrix} \tag{17}$$

From Eq.(15); the Unitary Operator for the potential energy portion, can be expressed as:

$$U_{\hat{x}}(t) = \mathbb{I} + \left(-\frac{it}{2}\right)^1 \frac{[m]}{1!} + \left(-\frac{it}{2}\right)^2 \frac{[m]^4}{2!} + \left(-\frac{it}{2}\right)^3 \frac{[m]^6}{3!} + ... \tag{18}$$

Where; m = $\hat{x}^d$. We can observe an exact Taylor expansion of the exponential function formed by the addition of the corresponding diagonal elements of the matrix $U_{\hat{x}}$ (after expanding the above expression). We also notice that it is symmetrical about the element at position [16, 16] which is

unity.

$$U_{\hat{x}}(t) = \begin{bmatrix} e^{-6.29it} & 0 & 0\ 0\ .\ . & . & 0 \\ 0 & e^{-5.52it} & 0\ 0\ .\ . & . & 0 \\ 0 & 0 & 0\ .\ .\ . & . & 0 \\ . & . & .\ .\ .\ . & . & . \\ 0 & 0 & 0\ 0\ .\ . & e^{-4.81it} & 0 \\ 0 & 0 & 0\ 0\ .\ . & 0 & e^{-5.52it} \end{bmatrix} \tag{19}$$

$U_{\hat{x}}(t)[1,1]$	1 - 6.29it - $19.76t^2 + ...$	exp(-6.29it)
$U_{\hat{x}}(t)[2,2]$	1 - 5.52it - $15.26t^2 + ...$	exp(-5.52it)
$U_{\hat{x}}(t)[3,3]$	1 - 4.81it - $11.58t^2 + ...$	exp(-4.81it)
.	.....	.
.	.....	.
.	.....	.
.	.....	.
$U_{\hat{x}}(t)[31,31]$	1 - 4.81it - $11.58t^2 + ...$	exp(-4.81it)
$U_{\hat{x}}(t)[32,32]$	1 - 5.52it - $15.26t^2 + ...$	exp(-5.52it)

TABLE II. Taylor Expansion of Exponential function in $U_{\hat{x}}$.

Now we factor out the element at position [1,1] from the above equation (which kind of acts as a global phase) and we get the ultimate form for the unitary operator as:

$$U_{\hat{x}}(t) = e^{-6.29it} \begin{bmatrix} 1 & 0 & 0\ 0\ .\ . & . & 0 \\ 0 & e^{0.77it} & 0\ 0\ .\ . & . & 0 \\ 0 & 0 & 0\ .\ .\ . & . & 0 \\ . & . & .\ .\ .\ . & . & . \\ 0 & 0 & 0\ 0\ .\ . & e^{1.48it} & 0 \\ 0 & 0 & 0\ 0\ .\ . & 0 & e^{0.77it} \end{bmatrix} \tag{20}$$

From the above matrix; we can see that the first diagonal element is independent of any phase term and hence gives an upper edge in the formation of quantum circuit. The rest of the diagonal terms hold the phase values to be provided to the next 31 basis states in the sequence. Therefore, the complete Unitary Operator for our case can be given as:

$$U(t) = exp\left[\left(-\frac{it}{2}\right)(\hat{p}_x^2 + \hat{p}_y^2 + \hat{x}^2 + \hat{y}^2)\right] = U_{\hat{p}_x} U_{\hat{p}_y} U_{\hat{x}} U_{\hat{y}} \tag{21}$$

The orthogonality of the spatial dimensions x and y makes it possible that they obey the same mathematical procedure independently.

GENERALIZATION

The Momentum and Position Operators are orthogonal so they commute with each other which further allows us to generalize our methodology for computing the unitary operator to any arbitrary

spatial dimensions. Here we will generalize the calculation of unitary operator for any arbitrary state using any arbitrary number of qubits. The following matrices and tables are relevant for the same:

$$[\hat{x}^d] = \sqrt{\frac{2\pi}{N}} \begin{bmatrix} -N/2 & 0 & 0 \; . \; . & 0 \\ 0 & (-N/2)+1 & 0 \; . \; . & 0 \\ . & . & . \; . \; . & . \\ 0 & 0 & . \; . \; . & . \\ 0 & 0 & 0 \; . \; 0 & (N/2)-1 \end{bmatrix} \tag{22}$$

$$[\hat{x}^d]^2 = [\hat{x}^d]' = \left(\frac{2\pi}{N}\right) \begin{bmatrix} (-N/2)^2 & 0 & 0 \; . & 0 \\ 0 & ((-N/2)+1)^2 & 0 \; . & 0 \\ . & . & . \; . & . \\ 0 & 0 & . \; . & . \\ 0 & 0 & 0 \; . & ((N/2)-1)^2 \end{bmatrix} \tag{23}$$

And the Unitary Operator will be:

$$U(t) = exp\Big[- \frac{i[\hat{x}^d]^2 t}{2} \Big]$$

Which can be written/ expanded using Taylor expansion as:

$$U(t) = exp\Big[- \frac{it[\hat{x}^d]^2}{2} \Big] = \mathbb{I} + \sum_{m=1}^{\infty} \left(- \frac{it}{2} \right)^m \frac{[[\hat{x}^d]^2]^m}{m!}$$

$$\implies U_{\hat{x}}(t) = \mathbb{I} + \left(- \frac{it}{2} \right)^1 \frac{[\hat{x}^d]^2}{1!} + \left(- \frac{it}{2} \right)^2 \frac{[\hat{x}^d]^4}{2!} + \left(- \frac{it}{2} \right)^3 \frac{[\hat{x}^d]^6}{3!} + ... \tag{24}$$

To avoid Mathematical complexity and to give the jest of the algorithm, we will drop the term $\left(\frac{2\pi}{N}\right)$ and write the Unitary operator in its matrix form:

$$U_{\hat{x}}(t) = \begin{bmatrix} e^{(-\frac{N}{2})^2 it} & 0 & 0 \; . \; . & . & 0 \\ 0 & e^{((-\frac{N}{2})+1)^2 it} & 0 \; . \; . & . & 0 \\ . & . & . \; . \; . & . & . \\ 0 & 0 & 0 \; 0 \; . & e^{((-\frac{N}{2})-2)^2 it} & 0 \\ 0 & 0 & 0 \; 0 \; . & 0 & e^{((-\frac{N}{2})-1)^2 it} \end{bmatrix} \tag{25}$$

6. CIRCUIT IMPLEMENTATION

Using Eq.(21), we can naturally figure out that by making a circuit for $U_x(t)$ and $U_p(t)$ in series, we can complete the quantum circuit for the complete Unitary operator. Initially we will implement

$U_p(t)$ because $U_x(t)$ simply adds the extra phase factor in the circuit. And also to implement $U_p(t)$ we need the Quantum Fourier Transform. So, we first propose a generalized circuit for Quantum Fourier Transform[3] in Fig.(2) which is given in the next page.
Before that we must consider that the basis states enumerate all the possible states of the qubits given as:

$$|x\rangle = |x_1 x_2 \dots x_n\rangle = |x_1\rangle \otimes |x_2\rangle \otimes \cdots \otimes |x_n\rangle \tag{26}$$

Where, with tensor product notation '$\otimes$', $|x_j\rangle$ indicates that qubit j is in state x_j, with x_j either 0 or 1.

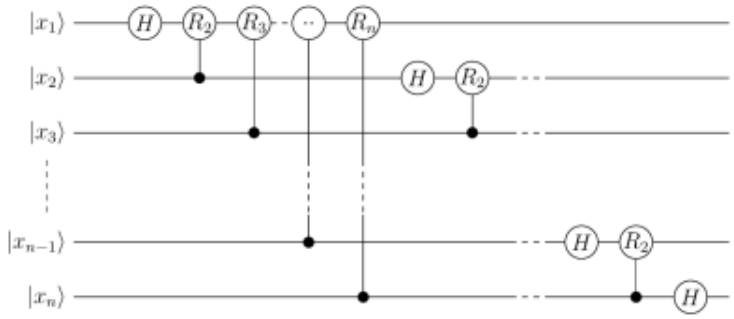

Figure 2. A generalized circuit for the implementation of The Quantum Fourier Transform of n-qubit system.

In the above circuit, the quantum gates used are Hadamard Gate (H) and Controlled Phase Gate (R_m). An efficient quantum circuit for Quantum Fourier Transform of a 5-qubit system is given in Fig.(3) in the next page. The phase of the individual controlled U1 gate is given by:

$$\phi = \frac{2\pi}{2^n}$$

Here, n = number of qubits used in the system. The controlled phase gate (cU1) can thus be written in the form of a matrix:

$$cU1_n = \begin{bmatrix} 1 & 0 \\ 0 & e^{\frac{2\pi i}{2^n}} \end{bmatrix} \tag{27}$$

With $e^{\frac{2\pi i}{2^n}} = \omega'_n = \omega_{(2^n)}$ which further indicates that $\omega_{(2^n)}$ or ω'_n is the primitive 2^n-th root of unity (or 1).
So, we express H and $cU1_n$ in terms of:

$$H = \frac{1}{\sqrt{2}} \begin{bmatrix} 1 & 1 \\ 1 & -1 \end{bmatrix} \qquad \text{and} \qquad cU1_n = \begin{bmatrix} 1 & 0 \\ 0 & e^{\frac{2\pi i}{2^n}} \end{bmatrix} \tag{28}$$

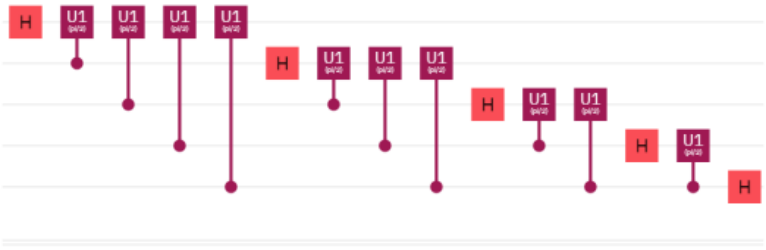

Figure 3. A circuit for implementing the Quantum Fourier Transform using 5-qubit system.

Similarly, in order to implement the inverted Quantum Fourier Transform (QFT), we need to generate a quantum circuit which is the mirror image of Quantum Fourier Transform with conjugate phases at each controlled phase gate. An efficient quantum circuit for the same is given in Fig.(4).

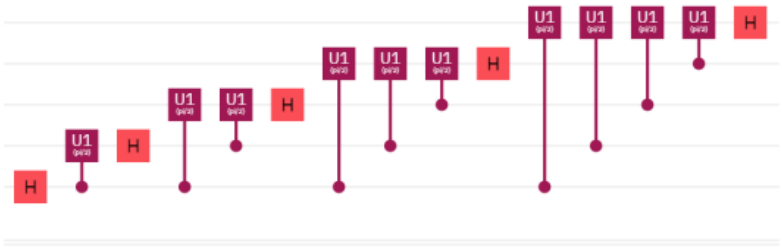

Figure 4. A circuit depicting the Inverted QFT-Modified Mirror image of the circuit for direct Quantum Fourier Transform.

Now the operator $[x^d]'$ which comes in between the QFT and inverted QFT, can be implemented by using a series of Toffolli gate (also known as CCNOT gate or $D(\pi/2)$ gate) and Controlled Phase gate. To make the circuit applicable for all possible states of a 5-qubit system, we need to make circuit in such a way that each of the state kind of gets the correct phase and provides an accurate result. Here, we kind of make the quantum circuit (which is also called a filter) in the specific fashion that the crucial phase information has been imparted. Each set of filters form the state for the next set of filter and a series of such 31 filters can be used recursively to implement all the 31 phase rotations to achieve $U_x(t)$ (or to reduce the number of gates, one can exploit the symmetry about the element positioned at [16,16] by using controlled X gate). A filter for the first state 00001 is illustrated in Fig.(5).

Now by using the same technique, we can prepare the basic quantum circuit for a 3-qubit system. First, we will write the unitary matrix for a 3-qubit system and then we will expand each diagonal element of the unitary operator to make an exact Taylor expansion of the exponential function.

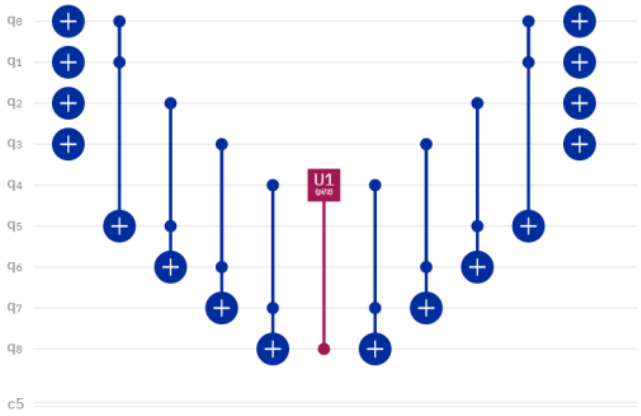

Figure 5. The Inverted QFT-Modified Mirror image of Circuit For Direct Quantum Fourier Transform.

The following matrix is the unitary operator for the 3-qubit system:

$$U_x^3(t) = \begin{bmatrix} e^{-1.57it} & 0 & 0 & 0 \ldots & 0 \\ 0 & e^{-0.88it} & 0 & 0 \ldots & 0 \\ 0 & 0 & e^{-0.39it} & \ldots & 0 \\ . & . & . & \ldots & . \\ 0 & 0 & 0 & 0 \ldots e^{-0.39it} & 0 \\ 0 & 0 & 0 & 0 \ldots 0 & e^{-0.88it} \end{bmatrix}$$

$$\implies U_x^3(t) = e^{-1.57it} \begin{bmatrix} 1 & 0 & 0 & 0 \ldots & 0 \\ 0 & e^{0.69it} & 0 & 0 \ldots & 0 \\ 0 & 0 & e^{1.18it} & \ldots & 0 \\ . & . & . & \ldots & . \\ 0 & 0 & 0 & 0 \ldots e^{1.18it} & 0 \\ 0 & 0 & 0 & 0 \ldots 0 & e^{0.69it} \end{bmatrix} \tag{29}$$

Now, clearly by using the quantum Fourier transform and its inverse with our filters in between, we can design and implement the circuit for 3-qubit system. And, U3 gates can be used in the very beginning of the circuit to initialize the circuit to some arbitrary state.
The quantum circuit for the 3-qubit system is shown in Fig.(6).

Figure 6. Quantum circuit for implementing $U_p(t)$ for a 3-qubit system.

7. IMPLEMENTATION ON A BOSONIC SYSTEM

The Hamiltonian of the full system is given by[5]:

$$\hat{H} = \hat{H}_{field} + \hat{H}_{atom} + \hat{H}_{int}$$

where $\hat{H}_{field}$ is the free Hamiltonian, $\hat{H}_{atom}$ is the atomic excitation Hamiltonian and $\hat{H}_{int}$ is the interaction Hamiltonian.

7.1 *MODEL*

We can derive the Pauli Matrix Equivalents for Bosonic System by using the following three equations[6]:

$$(\sigma_3)_{jl} = \frac{\langle s, j|S_k|s, l\rangle}{s\hbar} = \frac{j}{s}\delta_{ij} \tag{30}$$

$$(\sigma_1)_{j\,l} = \frac{[s\,(s+1) - j\,(j-1)]^{1/2}}{2\,s}\,\delta_{j\;l+1} + \frac{[s\,(s+1) - j\,(j+1)]^{1/2}}{2\,s}\,\delta_{j\;l-1} \tag{31}$$

$$(\sigma_2)_{j\,l} = \frac{[s\,(s+1) - j\,(j-1)]^{1/2}}{2\,\mathrm{i}\,s}\,\delta_{j\;l+1} - \frac{[s\,(s+1) - j\,(j+1)]^{1/2}}{2\,\mathrm{i}\,s}\,\delta_{j\;l-1} \tag{32}$$

$\therefore$ By using the above three equations, we have:

$$\sigma_1 = \frac{1}{\sqrt{2}}\begin{bmatrix} 0 & 1 & 0 \\ 1 & 0 & 1 \\ 0 & 1 & 0 \end{bmatrix} \tag{33}$$

$$\sigma_2 = \frac{1}{\sqrt{2}}\begin{bmatrix} 0 & -i & 0 \\ i & 0 & -i \\ 0 & i & 0 \end{bmatrix} \tag{34}$$

$$\sigma_3 = \begin{bmatrix} 1 & 0 & 0 \\ 0 & 0 & 0 \\ 0 & 0 & -1 \end{bmatrix} \tag{35}$$

Where, $\sigma_1, \sigma_2, \sigma_3$ are the Pauli Matrix equivalents for Bosonic particles.

We have modeled our system using Rabi Hamiltonian. However, in our case we will be using somewhat modified version of Rabi Hamiltonian[7]:

$$H_s = \sum_{k=1}^{2} \omega_k b_k^\dagger b_k + \frac{\omega_0}{2}\sigma_3 + \sum_{k=1}^{2} g_k(e^{i\theta_k} b_k + e^{-i\theta_k} b_k^\dagger)\sigma_1 \tag{36}$$

Where ω_0 is the frequency of the main oscillator, ω_k is the frequency of the k-th environment oscillator; $b_k^\dagger$ and b_k are the creation and annihilation operators of the main system and the k-th environmental oscillator respectively. Whereas g_k's are the coupling constant for the interaction between the k-th environment oscillator and the main quantum oscillator. We set k=1 from now to prevent us from complicating the process.
For simplicity, we will consider the simplest case of our model and substitute k=1 in our original Hamiltonian [in Eq.(36)] to obtain the special case of our Hamiltonian which will be our working Hamiltonian from now:

$$H = \omega_1 b_1^\dagger b_1 + \frac{\omega_0}{2}\sigma_3 + g_1(e^{i\theta_1} b_1 + e^{-i\theta_1} b_1^\dagger)\sigma_1$$

For simplicity we will drop the sub-script 1 from our Hamiltonian and obtain:

$$H = \omega b^\dagger b + \frac{\omega_0}{2}\sigma_3 + g(e^{i\theta} b + e^{-i\theta} b^\dagger)\sigma_1 \tag{37}$$

7.2 *RELEVANT TRANSFORMATION AND GENERALIZATION*

Now, as our system involves Bosonic particles, so the following commutation relations uphold:

$$[b_i, b_j^\dagger] \equiv b_i b_j^\dagger - b_j^\dagger b_i = \delta_{ij} \tag{38}$$

$$[b_i^\dagger, b_j^\dagger] = [b_i, b_j] = 0 \tag{39}$$

Here δ_{ij} is known as 'Kronecker delta'.
The operators used in the Hamiltonian can be transformed according to Holstein-Primakoff transformations (i.e. it maps spin operators for a system of spin-S moments on a lattice to creation and annihilation operators) as[8]:

$$\hat{S}_j^+ = \sqrt{(2S - \hat{n}_j)}\hat{b}_j \tag{40}$$

$$\hat{S}_j^- = \hat{b}_j^\dagger \sqrt{(2S - \hat{n}_j)} \tag{41}$$

Where $\hat{b}_j^\dagger$ ($\hat{b}_j$) is the creation (annihilation) operator at site j that satisfies the commutation relations mentioned above and $\hat{n}_j = \hat{b}_j^\dagger \hat{b}_j$ is the "Number Operator". Hence we can generalize the above equations as:

$$S^+ = \sqrt{(2S - b^\dagger b)}b \tag{42}$$

$$S^- = b^\dagger \sqrt{(2S - b^\dagger b)} \tag{43}$$

Where;

$$S_+ \equiv S_x + iS_y \qquad \text{and} \qquad S_- \equiv S_x - iS_y$$

Where; S_x (= σ_1), S_y (= σ_2), S_z (= σ_3) are the Pauli matrices for Bosonic system (as mentioned in the previous section).
Now by using the above transformations; we can write our creation and annihilation operators in terms of Matrices as:

$$b^\dagger = \begin{bmatrix} 0 & 0 & 0 \\ 1 & 0 & 0 \\ 0 & 1 & 0 \end{bmatrix} \qquad \text{and} \qquad b = \begin{bmatrix} 0 & 1 & 0 \\ 0 & 0 & 1 \\ 0 & 0 & 0 \end{bmatrix} \tag{44}$$

Now the Hamiltonian for our coupled Quantum Harmonic Oscillator in Eq.(37) can be decomposed as:

$$H = \omega b^\dagger b \otimes \mathbb{I} + \frac{\omega_0}{2} \mathbb{I} \otimes \sigma_3 + g(e^{i\theta} b + e^{-i\theta} b^\dagger) \otimes \sigma_1$$

Or the above equation can be written as:

$$H = \omega b^\dagger b \otimes \mathbb{I} + \frac{\omega_0}{2} \mathbb{I} \otimes S_3 + g(e^{i\theta} b + e^{-i\theta} b^\dagger) \otimes S_1 \tag{45}$$

Now, we will evaluate each term to simplify the expression of the Hamiltonian in the form of matrix. Here,

$$\omega b^\dagger b \otimes \mathbb{I} = \omega \begin{bmatrix} 0 & 0 & 0 \\ 0 & 1 & 0 \\ 0 & 0 & 1 \end{bmatrix} \otimes \begin{bmatrix} 1 & 0 & 0 \\ 0 & 1 & 0 \\ 0 & 0 & 1 \end{bmatrix}$$

$$\Rightarrow \omega b^\dagger b \otimes \mathbb{I} = \begin{bmatrix} 0 & 0 & 0 & 0 & 0 & 0 & 0 & 0 & 0 \\ 0 & 0 & 0 & 0 & 0 & 0 & 0 & 0 & 0 \\ 0 & 0 & 0 & 0 & 0 & 0 & 0 & 0 & 0 \\ 0 & 0 & 0 & \omega & 0 & 0 & 0 & 0 & 0 \\ 0 & 0 & 0 & 0 & \omega & 0 & 0 & 0 & 0 \\ 0 & 0 & 0 & 0 & 0 & \omega & 0 & 0 & 0 \\ 0 & 0 & 0 & 0 & 0 & 0 & \omega & 0 & 0 \\ 0 & 0 & 0 & 0 & 0 & 0 & 0 & \omega & 0 \\ 0 & 0 & 0 & 0 & 0 & 0 & 0 & 0 & \omega \end{bmatrix} \tag{46}$$

Similarly,

$$\frac{\omega_0}{2}\mathbb{I}\otimes S_z=\frac{\omega_0}{2}\begin{bmatrix}1&0&0\\0&1&0\\0&0&1\end{bmatrix}\otimes\begin{bmatrix}1&0&0\\0&0&0\\0&0&-1\end{bmatrix}$$

$$\Rightarrow \frac{\omega_0}{2}\mathbb{I}\otimes S_z=\begin{bmatrix}\frac{\omega_0}{2}&0&0&0&0&0&0&0&0\\0&0&0&0&0&0&0&0&0\\0&0&-\frac{\omega_0}{2}&0&0&0&0&0&0\\0&0&0&\frac{\omega_0}{2}&0&0&0&0&0\\0&0&0&0&0&0&0&0&0\\0&0&0&0&0&-\frac{\omega_0}{2}&0&0&0\\0&0&0&0&0&0&\frac{\omega_0}{2}&0&0\\0&0&0&0&0&0&0&0&0\\0&0&0&0&0&0&0&0&-\frac{\omega_0}{2}\end{bmatrix} \tag{47}$$

Finally,

$$g(e^{i\theta}b+e^{-i\theta}b^\dagger)\otimes S_x=\frac{g}{\sqrt{2}}\begin{bmatrix}0&e^{i\theta}&0\\e^{-i\theta}&0&e^{i\theta}\\0&e^{-i\theta}&0\end{bmatrix}\otimes\begin{bmatrix}0&1&0\\1&0&1\\0&1&0\end{bmatrix}$$

$$\Rightarrow g(e^{i\theta}b+e^{-i\theta}b^\dagger)\otimes S_x=\frac{g}{\sqrt{2}}\begin{bmatrix}0&0&0&0&e^{i\theta}&0&0&0&0\\0&0&0&e^{i\theta}&0&e^{i\theta}&0&0&0\\0&0&0&0&e^{i\theta}&0&0&0&0\\0&e^{-i\theta}&0&0&0&0&0&e^{i\theta}&0\\e^{-i\theta}&0&e^{-i\theta}&0&0&0&e^{i\theta}&0&e^{i\theta}\\0&e^{-i\theta}&0&0&0&0&0&e^{i\theta}&0\\0&0&0&0&e^{-i\theta}&0&0&0&0\\0&0&0&e^{-i\theta}&0&e^{-i\theta}&0&0&0\\0&0&0&0&e^{-i\theta}&0&0&0&0\end{bmatrix} \tag{48}$$

Substituting the above values in Eq.(45), we get the value of H (a 9×9 matrix) as:

$$\Rightarrow H = \begin{bmatrix} \frac{\omega_0}{2} & 0 & 0 & 0 & \frac{ge^{i\theta}}{\sqrt{2}} & 0 & 0 & 0 & 0 \\ 0 & 0 & 0 & \frac{ge^{i\theta}}{\sqrt{2}} & 0 & \frac{ge^{i\theta}}{\sqrt{2}} & 0 & 0 & 0 \\ 0 & 0 & -\frac{\omega_0}{2} & 0 & \frac{ge^{i\theta}}{\sqrt{2}} & 0 & 0 & 0 & 0 \\ 0 & \frac{ge^{-i\theta}}{\sqrt{2}} & 0 & (\omega + \frac{\omega_0}{2}) & 0 & 0 & 0 & \frac{ge^{i\theta}}{\sqrt{2}} & 0 \\ \frac{ge^{-i\theta}}{\sqrt{2}} & 0 & \frac{ge^{-i\theta}}{\sqrt{2}} & 0 & \omega & 0 & \frac{ge^{i\theta}}{\sqrt{2}} & 0 & \frac{ge^{i\theta}}{\sqrt{2}} \\ 0 & \frac{ge^{-i\theta}}{\sqrt{2}} & 0 & 0 & 0 & (\omega - \frac{\omega_0}{2}) & 0 & \frac{ge^{i\theta}}{\sqrt{2}} & 0 \\ 0 & 0 & 0 & 0 & \frac{ge^{-i\theta}}{\sqrt{2}} & 0 & (\omega + \frac{\omega_0}{2}) & 0 & 0 \\ 0 & 0 & 0 & \frac{ge^{-i\theta}}{\sqrt{2}} & 0 & \frac{ge^{-i\theta}}{\sqrt{2}} & 0 & \omega & 0 \\ 0 & 0 & 0 & 0 & \frac{ge^{-i\theta}}{\sqrt{2}} & 0 & 0 & 0 & (\omega - \frac{\omega_0}{2}) \end{bmatrix}$$

8. DERIVATION OF UNITARY OPERATORS

Clearly, we know that for a system with Hamiltonian H, the unitary operator is given by:

$$U = e^{-iHt} \tag{49}$$

Where H is the Hamiltonian of the system derived in the previous section.
But to find the unitary operator compatible, we need to change the form of our Hamiltonian and write it as a sum of two matrices whose corresponding unitary operators are relatively easier to compute:

$$H = X + Y$$

Where,

$$X = \begin{bmatrix} \frac{\omega_0}{2} & 0 & 0 & 0 & 0 & 0 & 0 & 0 & 0 \\ 0 & 0 & 0 & 0 & 0 & 0 & 0 & 0 & 0 \\ 0 & 0 & -\frac{\omega_0}{2} & 0 & 0 & 0 & 0 & 0 & 0 \\ 0 & 0 & 0 & (\omega + \frac{\omega_0}{2}) & 0 & 0 & 0 & 0 & 0 \\ 0 & 0 & 0 & 0 & \omega & 0 & 0 & 0 & 0 \\ 0 & 0 & 0 & 0 & 0 & (\omega - \frac{\omega_0}{2}) & 0 & 0 & 0 \\ 0 & 0 & 0 & 0 & 0 & 0 & (\omega + \frac{\omega_0}{2}) & 0 & 0 \\ 0 & 0 & 0 & 0 & 0 & 0 & 0 & \omega & 0 \\ 0 & 0 & 0 & 0 & 0 & 0 & 0 & 0 & (\omega - \frac{\omega_0}{2}) \end{bmatrix}$$

$$Y = \begin{bmatrix} 0 & 0 & 0 & 0 & \frac{ge^{i\theta}}{\sqrt{2}} & 0 & 0 & 0 & 0 \\ 0 & 0 & 0 & \frac{ge^{i\theta}}{\sqrt{2}} & 0 & \frac{ge^{i\theta}}{\sqrt{2}} & 0 & 0 & 0 \\ 0 & 0 & 0 & 0 & \frac{ge^{i\theta}}{\sqrt{2}} & 0 & 0 & 0 & 0 \\ 0 & \frac{ge^{-i\theta}}{\sqrt{2}} & 0 & 0 & 0 & 0 & 0 & \frac{ge^{i\theta}}{\sqrt{2}} & 0 \\ \frac{ge^{-i\theta}}{\sqrt{2}} & 0 & \frac{ge^{-i\theta}}{\sqrt{2}} & 0 & 0 & 0 & \frac{ge^{i\theta}}{\sqrt{2}} & 0 & \frac{ge^{i\theta}}{\sqrt{2}} \\ 0 & \frac{ge^{-i\theta}}{\sqrt{2}} & 0 & 0 & 0 & 0 & 0 & \frac{ge^{i\theta}}{\sqrt{2}} & 0 \\ 0 & 0 & 0 & 0 & \frac{ge^{-i\theta}}{\sqrt{2}} & 0 & 0 & 0 & 0 \\ 0 & 0 & 0 & \frac{ge^{-i\theta}}{\sqrt{2}} & 0 & \frac{ge^{-i\theta}}{\sqrt{2}} & 0 & 0 & 0 \\ 0 & 0 & 0 & 0 & \frac{ge^{-i\theta}}{\sqrt{2}} & 0 & 0 & 0 & 0 \end{bmatrix}$$

Thus we have,

$$U = e^{-iXt}.e^{-iYt}$$
$$\implies U = U_x(t).U_y(t)$$

Where $U_x(t)$ = e^{-iXt} and $U_y(t)$ = e^{-iYt}. First we will compute $U_y(t)$, then $U_x(t)$. We can see that $U_y(t)$ can be expanded using Taylor series of expansion of the exponential function as:

$$U_y(t) = exp(-itY) = \mathbb{I} + \sum_{m=1}^{\infty}(-it)^m\frac{Y^m}{m!}$$
$$\implies U_y(t) = \mathbb{I} + (-it)^1\frac{Y}{1!} + (-it)^2\frac{Y^2}{2!} + (-it)^3\frac{Y^3}{3!} + (-it)^4\frac{Y^4}{4!} + (-it)^5\frac{Y^5}{5!} + ...$$

Now, for simplicity, let us denote $\frac{g}{\sqrt{2}}$ = $g^{'}$. So, we have:

$$\implies U_y(t) = [1+\frac{(-itg^{'})^2}{2!}+\frac{(-itg^{'})^4}{4!}+...]\mathbb{I}+[\frac{(-itg^{'})}{1!}+\frac{(-itg^{'})^3}{3!}+\frac{(-itg^{'})^5}{5!}+...]M$$

Where;

$$M = \begin{bmatrix} 0 & 0 & 0 & 0 & e^{i\theta} & 0 & 0 & 0 & 0 \\ 0 & 0 & 0 & e^{i\theta} & 0 & e^{i\theta} & 0 & 0 & 0 \\ 0 & 0 & 0 & 0 & e^{i\theta} & 0 & 0 & 0 & 0 \\ 0 & e^{-i\theta} & 0 & 0 & 0 & 0 & 0 & e^{i\theta} & 0 \\ e^{-i\theta} & 0 & e^{-i\theta} & 0 & 0 & 0 & e^{i\theta} & 0 & e^{i\theta} \\ 0 & e^{-i\theta} & 0 & 0 & 0 & 0 & 0 & e^{i\theta} & 0 \\ 0 & 0 & 0 & 0 & e^{-i\theta} & 0 & 0 & 0 & 0 \\ 0 & 0 & 0 & e^{-i\theta} & 0 & e^{-i\theta} & 0 & 0 & 0 \\ 0 & 0 & 0 & 0 & e^{-i\theta} & 0 & 0 & 0 & 0 \end{bmatrix}$$

(**We can observe that [Y^2, Y^4, Y^6,....] will give Identity matrices whereas [Y^1, Y^3, Y^5,...] will give the same matrix which is given above as M. So we differentiate them in two groups.)

$$\implies U_y(t) = \cos g^{'}t\mathbb{I} - iM\sin g^{'}t$$

$$\implies U_y(t) = \cos\frac{gt}{\sqrt{2}}\mathbb{I} - iM\sin\frac{gt}{\sqrt{2}} \tag{50}$$

Now for Bosonic particles, we need to use a 4-qubit system but for implementing a 4-qubit system we must require a 16×16 matrix because any matrix of order $N \times N$ must satisfy the condition $N = 2^n$ (where n= number of qubits). But we can express the above equation in form of a 16×16 matrix (which we have shown in the next sub-section), instead of a 9×9 matrix, by adding 1 diagonally seven times and placing 0 in other positions. In our situation we need only nine of the sixteen 4-qubit states (mentioned in Table (I)) because for the other seven states we will get the same Unitary matrix as result (i.e. without any change). We will use a 4-qubit system to simulate the above system. Therefore, we first note the results we get after operating $U_y(t)$ on different 4-qubit states so that we can go ahead on drawing the quantum circuit for the same.

Qubit states	Results after $U_y(t) acts$
$\|0000\rangle$	$(\cos\frac{gt}{\sqrt{2}}\|0000\rangle - i\sin\frac{gt}{\sqrt{2}}e^{-i\theta}\|0100\rangle)$
$\|0001\rangle$	$(\cos\frac{gt}{\sqrt{2}}\|0001\rangle - i\sin\frac{gt}{\sqrt{2}}e^{-i\theta}(\|0011\rangle + 0101))$
$\|0010\rangle$	$(\cos\frac{gt}{\sqrt{2}}\|0010\rangle - i\sin\frac{gt}{\sqrt{2}}e^{-i\theta}\|0100\rangle)$
$\|0011\rangle$	$(\cos\frac{gt}{\sqrt{2}}\|0011\rangle - i\sin\frac{gt}{\sqrt{2}}e^{-i\theta}\|0001\rangle - i\sin\frac{gt}{\sqrt{2}}e^{i\theta}\|0111\rangle)$
$\|0100\rangle$	$(\cos\frac{gt}{\sqrt{2}}\|0100\rangle - i\sin\frac{gt}{\sqrt{2}}e^{-i\theta}(\|0110\rangle + \|1000\rangle) - i\sin\frac{gt}{\sqrt{2}}e^{i\theta}(\|0000\rangle + \|0010\rangle))$
$\|0101\rangle$	$(\cos\frac{gt}{\sqrt{2}}\|0101\rangle - i\sin\frac{gt}{\sqrt{2}}e^{-i\theta}\|0111\rangle - i\sin\frac{gt}{\sqrt{2}}e^{i\theta}\|0001\rangle)$
$\|0110\rangle$	$(\cos\frac{gt}{\sqrt{2}}\|0110\rangle - i\sin\frac{gt}{\sqrt{2}}e^{i\theta}\|0100\rangle)$
$\|0111\rangle$	$(\cos\frac{gt}{\sqrt{2}}\|0111\rangle - i\sin\frac{gt}{\sqrt{2}}e^{i\theta}(\|0011\rangle + 0101))$
$\|1000\rangle$	$(\cos\frac{gt}{\sqrt{2}}\|1000\rangle - i\sin\frac{gt}{\sqrt{2}}e^{i\theta}\|0100\rangle)$

TABLE I. Operator $U_y(t)$ acting on Qubit States.

Now, we need to disentangle the final Quantum states after $U_y(t)$ Operator acts on the Qubit states

to be able to create the Quantum circuit. So, we can disentangle the final result as:

$$\left(\cos\frac{gt}{\sqrt{2}}0000 - \sin\frac{gt}{\sqrt{2}}e^{-i\theta}0100\right) = 0 \otimes \left(\cos\frac{gt}{\sqrt{2}}0 - \sin\frac{gt}{\sqrt{2}}e^{-i\theta}1\right) \otimes 0 \otimes 0$$

$$\vdots \qquad\qquad \vdots$$

$$\left(\cos\frac{gt}{\sqrt{2}}0110 - \sin\frac{gt}{\sqrt{2}}e^{i\theta}0100\right) = 0 \otimes 1 \otimes \left(\cos\frac{gt}{\sqrt{2}}1 - \sin\frac{gt}{\sqrt{2}}e^{i\theta}0\right) \otimes 0$$

$$\vdots \qquad\qquad \vdots$$

$$\left(\cos\frac{gt}{\sqrt{2}}1000 - \sin\frac{gt}{\sqrt{2}}e^{i\theta}0100\right) = \left(\cos\frac{gt}{\sqrt{2}}1 - \sin\frac{gt}{\sqrt{2}}e^{i\theta}0\right) \otimes 1 \otimes 0 \otimes 0$$

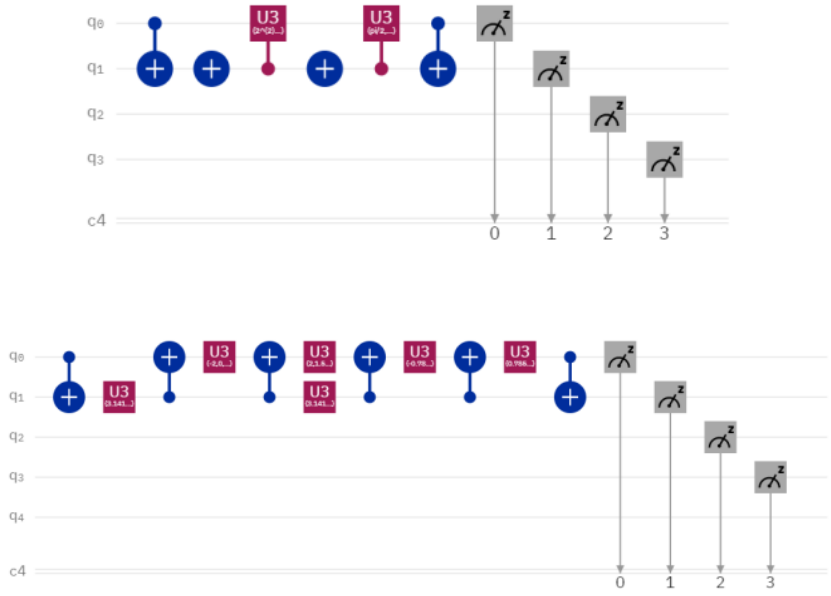

Figure 7. Filter for 1000 in case of $U_y(t)$ Operations

So, in the above segment, we computed the $U_y(t)$ operator and also disentangled the results. A filtered portion of our quantum circuit for the qubit state 1000 is shown in Fig.(7).
Now in order to compute $U_x(t)$ which is equal to e^{-iXt}, we first expand the expression using the Taylor expansion of the exponential function just like we did in earlier case as:

$$U_x(t) = exp(-itX) = \mathbb{I} + \sum_{m=1}^{\infty}(-it)^m\frac{X^m}{m!}$$

$$\implies U_x(t) = \mathbb{I} + (-it)^1 \frac{X}{1!} + (-it)^2 \frac{X^2}{2!} + (-it)^3 \frac{X^3}{3!} + (-it)^4 \frac{X^4}{4!} + (-it)^5 \frac{X^5}{5!} + ...$$

Therefore by using the above equation, we can express $U_x(t)$ in terms of e as:

$U_{\hat{x}}(t)[1,1]$	$\exp(-(\frac{\omega_0}{2})it)$
$U_{\hat{x}}(t)[2,2]$	$\exp(-(0)it)$
$U_{\hat{x}}(t)[3,3]$	$\exp((\frac{\omega_0}{2})it)$
$U_{\hat{x}}(t)[4,4]$	$\exp(-(\omega + \frac{\omega_0}{2})it)$
$U_{\hat{x}}(t)[5,5]$	$\exp(-(\omega)it)$
$U_{\hat{x}}(t)[6,6]$	$\exp(-(\omega - \frac{\omega_0}{2})it)$
$U_{\hat{x}}(t)[7,7]$	$\exp(-(\omega + \frac{\omega_0}{2})it)$
$U_{\hat{x}}(t)[8,8]$	$\exp(-(\omega)it)$
$U_{\hat{x}}(t)[9,9]$	$\exp(-(\omega - \frac{\omega_0}{2})it)$

In case of $U_x(t)$ Operator also; we will consider a 16×16 matrix (in place of a 9×9 matrix) because of same reason mentioned before and also we will construct the matrix in the same pattern as mentioned in case of $U_y(t)$ operator. It is easy to observe as X is a diagonal matrix, each diagonal element of $U_x(t)$ makes an exact Taylor expansion of the exponential function
(**The 16×16 matrix for both $U_y(t)$ and $U_x(t)$ operators are mentioned in the next sub-section.)
Again, we operate this operator on different 4-qubits states (in our situation we need only nine of the sixteen 4-qubit states because for the other seven states we will get the same Unitary matrix as result.) and then study the results for the same given in Table(II):
From the above table we can see the effect of $U_x(t)$ operator acting on the different 4-qubit states and we can construct the Quantum circuit for the same. A filtered portion of our quantum circuit for the qubit state 0000 is shown in Fig.(8).
Now, we know how to implement both the parts of our Unitary operator and the complete unitary matrix (16×16) can be implemented by operating both the operations in series. In this way we can easily calculate our Unitary operators for Bosonic system and also simulate the Unitary Operators for a Quantum Harmonic Oscillator. We present its simulation results on IBM quantum computer in the form of graphs later on. Each simulation is carried on IBMQ-qasm Simulator using 8192 shots for better accuracy.

Qubit states	Results after $\mathrm{U}_x(t) acts$
$\|0000\rangle$	$\mathrm{e}^{(-\frac{\omega_0}{2})it}\|0000\rangle$
$\|0001\rangle$	$\mathrm{e}^{(0)it}\|0000\rangle$
$\|0010\rangle$	$\mathrm{e}^{(\frac{\omega_0}{2})it}\|0000\rangle$
$\|0011\rangle$	$\mathrm{e}^{-(\omega+\frac{\omega_0}{2})it}\|0011\rangle$
$\|0100\rangle$	$\mathrm{e}^{(-\omega)it}\|0100\rangle$
$\|0101\rangle$	$\mathrm{e}^{-(\omega-\frac{\omega_0}{2})it}\|0101\rangle$
$\|0110\rangle$	$\mathrm{e}^{-(\omega+\frac{\omega_0}{2})it}\|0110\rangle$
$\|0111\rangle$	$\mathrm{e}^{(-\omega)it}\|0111\rangle$
$\|1000\rangle$	$\mathrm{e}^{-(\omega-\frac{\omega_0}{2})it}\|1000\rangle$

TABLE II. Operator $U_x(t)$ acting on Qubit States.

UNITARY OPERATOR MATRIX REPRESENTATIONS

The 16×16 Matrix representation of the Unitary operators $U_y(t)$ and $U_x(t)$ are:

$$U_y(t) = \begin{bmatrix}
A & 0 & 0 & 0 & B & 0 & 0 & 0 & 0 & 0 & 0 & 0 & 0 & 0 & 0 & 0 \\
0 & A & 0 & B & 0 & B & 0 & 0 & 0 & 0 & 0 & 0 & 0 & 0 & 0 & 0 \\
0 & 0 & A & 0 & B & 0 & 0 & 0 & 0 & 0 & 0 & 0 & 0 & 0 & 0 & 0 \\
0 & C & 0 & A & 0 & 0 & 0 & B & 0 & 0 & 0 & 0 & 0 & 0 & 0 & 0 \\
C & 0 & C & 0 & A & 0 & B & 0 & B & 0 & 0 & 0 & 0 & 0 & 0 & 0 \\
0 & C & 0 & 0 & 0 & A & 0 & B & 0 & 0 & 0 & 0 & 0 & 0 & 0 & 0 \\
0 & 0 & 0 & 0 & C & 0 & A & 0 & 0 & 0 & 0 & 0 & 0 & 0 & 0 & 0 \\
0 & 0 & 0 & C & 0 & C & 0 & A & 0 & 0 & 0 & 0 & 0 & 0 & 0 & 0 \\
0 & 0 & 0 & 0 & C & 0 & 0 & 0 & A & 0 & 0 & 0 & 0 & 0 & 0 & 0 \\
0 & 0 & 0 & 0 & 0 & 0 & 0 & 0 & 0 & 1 & 0 & 0 & 0 & 0 & 0 & 0 \\
0 & 0 & 0 & 0 & 0 & 0 & 0 & 0 & 0 & 0 & 1 & 0 & 0 & 0 & 0 & 0 \\
0 & 0 & 0 & 0 & 0 & 0 & 0 & 0 & 0 & 0 & 0 & 1 & 0 & 0 & 0 & 0 \\
0 & 0 & 0 & 0 & 0 & 0 & 0 & 0 & 0 & 0 & 0 & 0 & 1 & 0 & 0 & 0 \\
0 & 0 & 0 & 0 & 0 & 0 & 0 & 0 & 0 & 0 & 0 & 0 & 0 & 1 & 0 & 0 \\
0 & 0 & 0 & 0 & 0 & 0 & 0 & 0 & 0 & 0 & 0 & 0 & 0 & 0 & 1 & 0 \\
0 & 0 & 0 & 0 & 0 & 0 & 0 & 0 & 0 & 0 & 0 & 0 & 0 & 0 & 0 & 1
\end{bmatrix}$$

Where;

$$\mathrm{A} = \cos\left(\frac{gt}{\sqrt{2}}\right) \;\; ; \quad \mathrm{B} = -i\sin\left(\frac{gt}{\sqrt{2}}\right)e^{i\theta} \quad \text{and} \quad \mathrm{C} = -i\sin\left(\frac{gt}{\sqrt{2}}\right)e^{-i\theta}$$

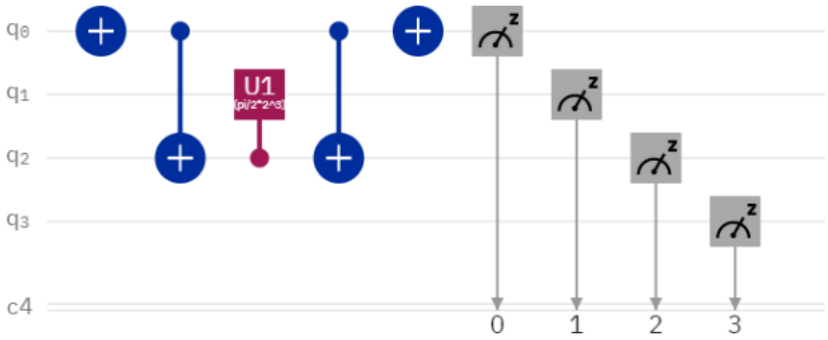

Figure 8. Filter for 0000 in case of $U_x(t)$ Operations

$$U_x(t) = \begin{bmatrix}
S & 0 & 0 & 0 & 0 & 0 & 0 & 0 & 0 & 0 & 0 & 0 & 0 & 0 & 0 & 0 \\
0 & 1 & 0 & 0 & 0 & 0 & 0 & 0 & 0 & 0 & 0 & 0 & 0 & 0 & 0 & 0 \\
0 & 0 & \frac{1}{S} & 0 & 0 & 0 & 0 & 0 & 0 & 0 & 0 & 0 & 0 & 0 & 0 & 0 \\
0 & 0 & 0 & P & 0 & 0 & 0 & 0 & 0 & 0 & 0 & 0 & 0 & 0 & 0 & 0 \\
0 & 0 & 0 & 0 & Q & 0 & 0 & 0 & 0 & 0 & 0 & 0 & 0 & 0 & 0 & 0 \\
0 & 0 & 0 & 0 & 0 & R & 0 & 0 & 0 & 0 & 0 & 0 & 0 & 0 & 0 & 0 \\
0 & 0 & 0 & 0 & 0 & 0 & P & 0 & 0 & 0 & 0 & 0 & 0 & 0 & 0 & 0 \\
0 & 0 & 0 & 0 & 0 & 0 & 0 & Q & 0 & 0 & 0 & 0 & 0 & 0 & 0 & 0 \\
0 & 0 & 0 & 0 & 0 & 0 & 0 & 0 & R & 0 & 0 & 0 & 0 & 0 & 0 & 0 \\
0 & 0 & 0 & 0 & 0 & 0 & 0 & 0 & 0 & 1 & 0 & 0 & 0 & 0 & 0 & 0 \\
0 & 0 & 0 & 0 & 0 & 0 & 0 & 0 & 0 & 0 & 1 & 0 & 0 & 0 & 0 & 0 \\
0 & 0 & 0 & 0 & 0 & 0 & 0 & 0 & 0 & 0 & 0 & 1 & 0 & 0 & 0 & 0 \\
0 & 0 & 0 & 0 & 0 & 0 & 0 & 0 & 0 & 0 & 0 & 0 & 1 & 0 & 0 & 0 \\
0 & 0 & 0 & 0 & 0 & 0 & 0 & 0 & 0 & 0 & 0 & 0 & 0 & 1 & 0 & 0 \\
0 & 0 & 0 & 0 & 0 & 0 & 0 & 0 & 0 & 0 & 0 & 0 & 0 & 0 & 1 & 0 \\
0 & 0 & 0 & 0 & 0 & 0 & 0 & 0 & 0 & 0 & 0 & 0 & 0 & 0 & 0 & 1
\end{bmatrix}$$

Where,

$$\text{P} = e^{-(\omega+\frac{\omega_0}{2})it}\ ; \quad \text{Q} = e^{(-\omega)it}\ ; \quad \text{R} = e^{-(\omega-\frac{\omega_0}{2})it}\ ; \quad \text{S} = e^{(-\frac{\omega_0}{2})it} \quad \text{and} \quad \frac{1}{s} = \frac{1}{e^{(-\frac{\omega_0}{2})it}} = e^{(\frac{\omega_0}{2})it}$$

9. RESULTS

In first part of our paper, we extend the idea of simulation of quantum harmonic oscillator by performing the simulation using higher number of qubits especially 5-qubits and we realized that we

are well able to do so using the IBMQ-qasm simulator present on the IBM Experience site. Our initial expectation was that taking higher number of qubits result in larger number of mesh points in the discretized space and hence results are produced with higher degree of accuracy in comparison with the system with lower number of qubits. We come to that result only after comparing data that we got during simulation using 3-qubit and 5-qubit system. The result of simulation of 3-qubit system is shown in Fig.(9).

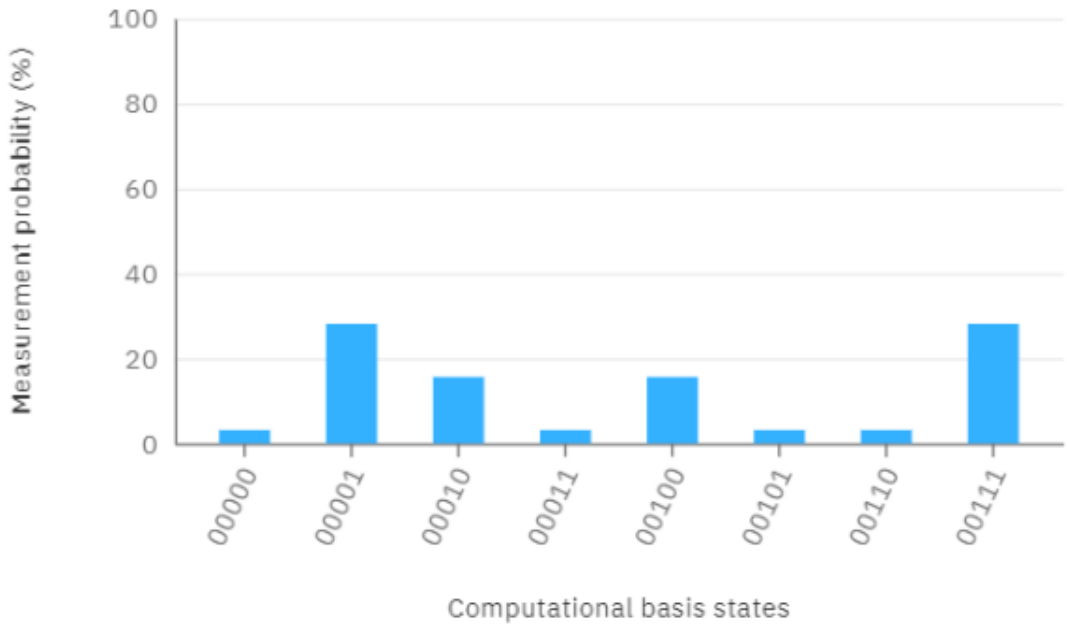

Figure 9. Graph between Measurement Probability vs Computational states in 3-qubit system.

In the final part of our paper, we use the idea of Pauli Matrices Equivalents for Bosonic particles and see the implementation of the equivalent matrices. Then we introduce a coupled Quantum Harmonic Oscillator to the Bosonic system and try to implement its Unitary Operator to the system using our previous section's knowledge and also simulate the Unitary Operators using IBMQ-experience (in 8192 shots for better accuracy). The Results of the simulation are shown in Fig.(10), Fig.(11) and Fig.(12) respectively.

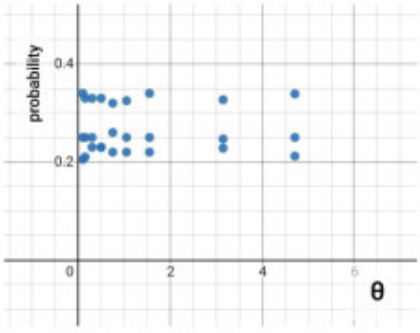

Figure 10. Graph between θ vs Probability

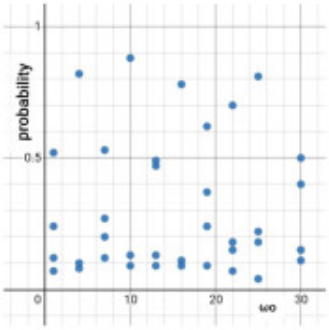

Figure 11. Graph between ω_0 vs Probability

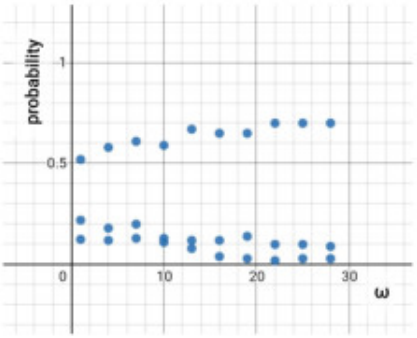

Figure 12. Graph between ω vs Probability

10. CONCLUSION

Now, we understand that the Quantum Harmonic Oscillator **(QHO)** is different from its classical counterpart in many aspects, so oscillation in classical case cannot be pictured in quantum realm. However, there is still something which is measurable and keeps the essence of Quantum Harmonic Oscillator alive. The measurable stuff that we are talking about is none other than the probability amplitudes of the states itself. From the simulations that we obtain on the IBMQ-Experience platform, it can be concluded that the variations of probability amplitudes of the states correspond to the oscillations in quantum sense. Moreover, by performing the simulations in two spacial dimensions, we can state that the results in each dimension is quite independent of the other which was expected intuitively. Clearly, for more accuracy, the number of qubits has to be increased and the generalization section of our work has to be used as it is valid for arbitrary number of qubits. In this project, we visualized the process for simulating a Quantum Harmonic Oscillator **(QHO)**, associated to a Bosonic system, using IBMQ-experience. In our case we derived the Unitary Operators for the **(QHO)** by using the Pauli Matrix equivalents for Bosonic system and after that we associated the usable Quantum States (4-qubit states) with the Unitary Operator (which is in-turn formed by

combining the $U_y(t)$ and $U_x(t)$ Operators in series). From the above process we can infer that the Unitary Operator is the sole factor which is necessary for simulating the **(QHO)** and we simulate the system by taking 8192 shots in IBMQ-experience because it will increase the effectiveness of our results and decrease the chance of any error in our simulation.

11. ACKNOWLEDGEMENTS

RT would like to thank Bikash K. Behera and Prof. Prasanta K. Panigrahi of Indian Institute of Science Education and Research, Kolkata for providing him guidance in this project. He also acknowledge the support of IBM Quantum Experience for producing experimental results and the results as well as views expressed are solely those of the author and do not reflect the official policy or position of IBM or the IBM Quantum Experience team.

References

[1] D. J. Griffths, Introduction to Quantum Mechanics, Pearson Prentice Hall (2004), URL: https://www.fisica.net/mecanica-quantica/Griffiths%20-%20Introduction%20to%20quantum%20mechanics.pdf

[2] Relation between Hamiltonian and the Operators, URL: https://en.wikipedia.org/wiki/Creation_and_annihilation_operators

[3] Quantum Fourier Transform, URL: https://en.wikipedia.org/wiki/Quantum_Fourier_transform

[4] V. K. Jain, B. K. Behera, and P. K. Panigrahi, Quantum Simulation of Discretized Harmonic Oscillator on IBMQuantum Computer, URL: https://www.researchgate.net/publication/334680969_Quantum_Simulation_of_Discretized_Harmonic_Oscillator_on_IBM_Quantum_Computer

[5] Jaynes-Cummings model, URL: https://en.wikipedia.org/wiki/Jaynes%E2%80%93Cummings_model

[6] Calculating the Pauli Matrix equivalent for Spin-1 Particles, URL: http://farside.ph.utexas.edu/teaching/qm/Quantum/node56.html

[7] B. Militello, H. Nakazato, and A. Napoli1, 2 : Synchronizing Quantum Harmonic Oscillators through Two-Level Systems, Phys. Rev. A **96**, 023862 (2017).

[8] Holstein-Primakoff transformation, URL: https://en.wikipedia.org/wiki/Holstein%E2%80%93Primakoff_transformation

Rainbow and Acid Rain

Sparsh Sinha[1], Rajesh B. Khaparde[2], Ajit M. Srivastava[3]

[1] UM-DAE Centre for Excellence in Basic Sciences, Mumbai 400098,
email: sparshsinha30101998k@gmail.com
[2] Homi Bhabha Centre for Science Education, TIFR, Mumbai 400088, email: rajesh@hbcse.tifr.res.in
[3] Institute of Physics, Bhubaneswar 751005, email: ajit@iopb.res.in

Abstract: This experimental study investigates the possibility of measurement of rainbow angle and using it to get an estimate of the acidity or pH of rainwater falling at a distant place. We studied the rainbow angle in the laboratory using a pendent drop of a liquid, and measured the total angle of deviation for the first and the second order rainbow for various values of pH of the acidic solution. We used sulfuric acid and nitric acid which make up most of the acid rain. In the case of sulfuric acid, the variation was found to be 1.202° and 2.074° for angle of deviation corresponding to first and second order rainbow, respectively. In case of nitric acid, the variation in angle of deviation corresponding to first order and second order rainbow was found to be 0.376° and 1.507°, respectively. The experimental results show that there is small change in the rainbow angle with variation of pH of the acidic solution of the drop.

Keywords: Rainbow, acid rain, refractive index, acidity (pH) measurement

1. INTRODUCTION

Rainbow is one of the most beautiful phenomena observed in nature. On a rainy day, a rainbow is produced when white light from the sun falls and gets deviated to the eyes of an observer on the earth due to a large number of raindrops in the sky (Figure 1).

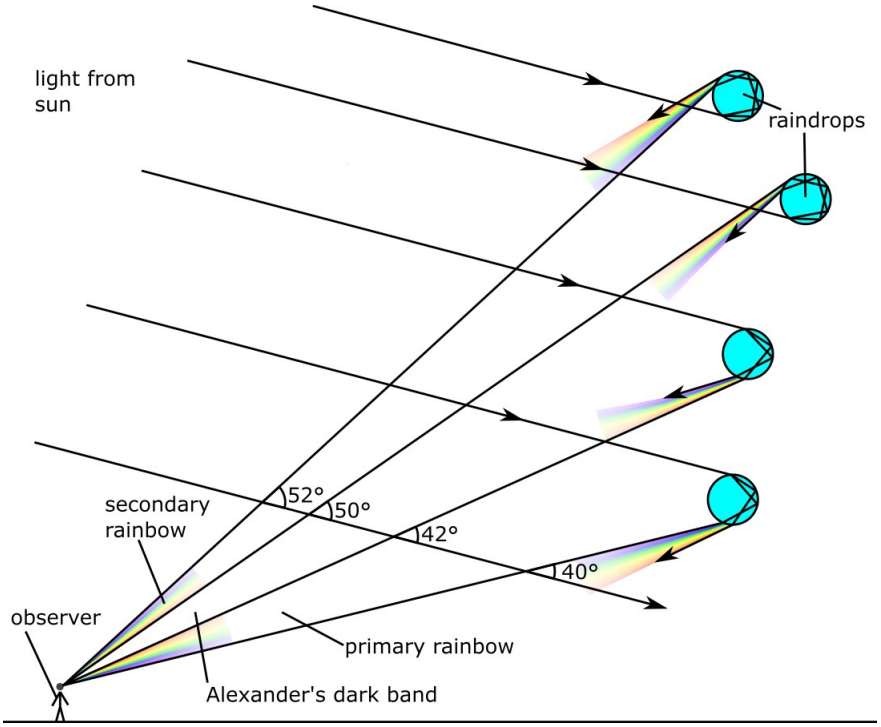

Figure 1: Formation of primary (first order) and secondary (second order) rainbow

The several colors in a rainbow are due to the fact that sunlight is made up of a range of colors, and the light of different colors is refracted at different angles, when it passes from one medium into another. Thus 'dispersion' occurs as sunlight propagates through the drop. From the surface of the earth, we can easily observe primary (first order) and secondary (second order) rainbows and the Alexander's dark band between the two rainbows.

Acid rain results when sulfur dioxide (SO_2) and nitrogen oxides (NO_x) present in the atmosphere get absorbed in the precipitating rainwater [1]. The acids (having different refractive indices) and their interaction with water molecules together contribute to the change in the refractive index of rainwater, which affect the angle (with respect to the incident sunlight) at which the rainbow is observed.

The relation between the angle of deviation for different order rainbows and refractive index of the liquid is well defined in geometrical optics [2]. There exists almost a linear relation between refractive index and low concentrations of acid in solutions [3], [4], and these concentrations can be determined using pH in the range of 0 to 7, hence it is possible to show the variation of angle of deviation of different order rainbow with the pH. This provides a possibility that the measurement of rainbow angle can be used to estimate the acidity of rainwater falling at a distant place. We conducted a systematic study of this possibility using a single droplet in a laboratory. We studied the variation of the angle at which rainbow is observed by using a drop of acidic solution with varying pH of the drop.

In this laboratory investigation on formation of rainbow with acidic solutions, we use a red He-Ne laser as a source of parallel beam of monochromatic light. Here, we do not observe various colors as in the case of a rainbow in the sky formed due to sunlight falling on the water drops. We still use the term 'rainbow' that here refers to the first bright fringe (from a set of fringes) emerging from a pendent drop of a liquid which is observed through the telescope of a prism spectrometer.

2. THEORY

In view of geometrical optics, a rainbow formation takes place because of a ray getting reflected and refracted in a droplet of water with refractive index μ. Consider Figure 2 for the first order rainbow (k = 1) formed because of a spherical droplet with a single ray. If we follow along the path of the ray, we find that the ray undergoes a refraction then an internal reflection and finally a refraction emerging at C. If i and r be the angle of incidence and the angle of refraction respectively, and if φ_1 is the total angle of deviation of the emerging ray from the ray incident on the drop then,

$$\varphi_1 = 180° + 2i - 4r$$

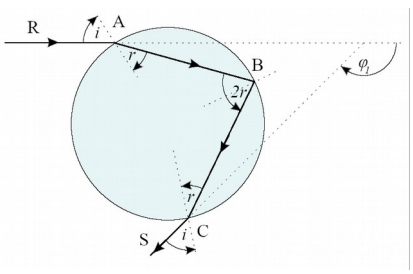

Figure 2: Ray diagram for the first order rainbow formed from a spherical drop

For the second order rainbow instead of one internal reflection there are two internal reflections as shown in Figure 3 and if φ_2 is the total angle of deviation of the emerging ray from the ray incident on the drop then,

$\varphi_2 = 360° + 2i - 6r$

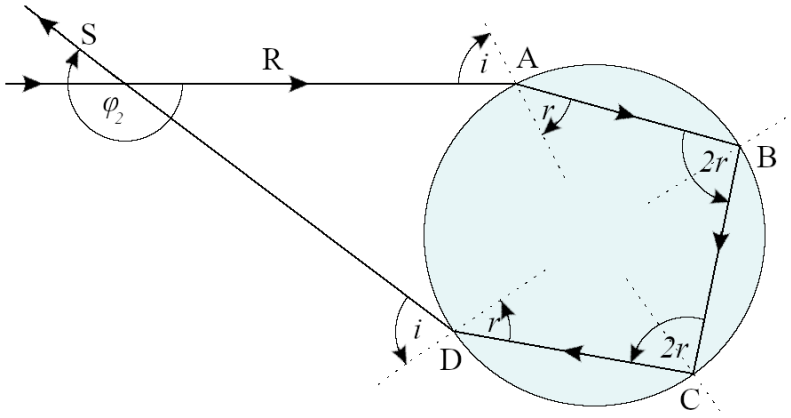

Figure 3: Ray diagram for the second order rainbow formed from a spherical drop

In the same manner, for k[th] order rainbow, as derived in [5], if φ_k is the total angle of deviation of the emerging ray from the ray incident on the drop then,

$\varphi_k = 180k + 2i - 2(k+1)r$

We minimize φ_k with respect to angle i (and use Snell's law), for finding the minimum angle of deviation at which rainbow formation takes place. We find the minimum φ_k to be:

$$\varphi_k = 180k + 2\cos^{-1}\sqrt{\frac{\mu^2-1}{k(k+2)}} - 2(k+1)\sin^{-1}\left(\frac{\sin\cos^{-1}\sqrt{\frac{\mu^2-1}{k(k+2)}}}{\mu}\right) \qquad \text{....(Eq. 1)}$$

We plotted using Desmos [6], a theoretically expected graph of variation of total angle of deviation or rainbow angle φ_k as given by equation (1) with refractive index μ for various orders of rainbow i.e., k = 1, 2, 3, 4 and 5 as shown in Figure 4.

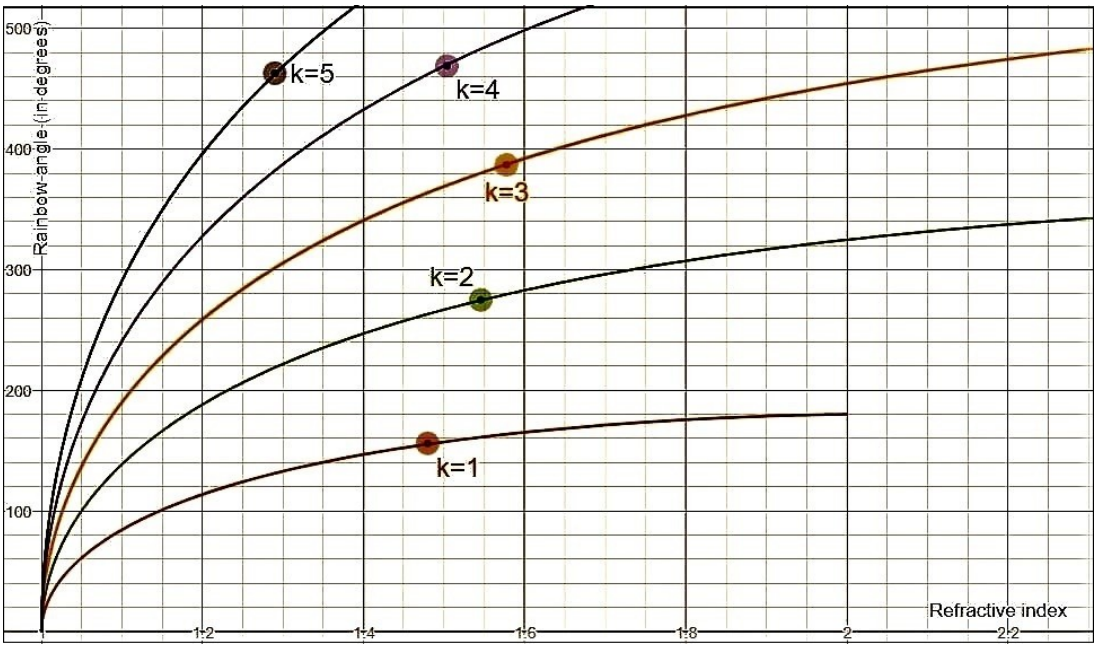

Figure 4: Plot of variation of rainbow angle φ_k with refractive index μ for various values of k

3. EXPERIMENTAL SETUP

The complete experimental arrangement is as shown in Figure 5 and Figure 6. The experimental setup used in this study consisted of the following main components:

(a) A He-Ne red laser source (wavelength 632.8 nm with 5 mW of power) was used as a source of monochromatic and parallel beam of light. The laser source was mounted on a precision laboratory jack using a laser mount as shown in Figure 6.

(b) A prism spectrometer (9 inches diameter scale and having least count of 0.0028°, Make: Optiregion [7]) was used for measuring the angle of deviation for the first and second order rainbows. A specially designed mount with a syringe holder was used for holding the syringe on the prism table of the spectrometer. At the front (where light enters) of the collimator an aluminum sheet with a hole of 2 mm diameter, was stuck using foam tape. Lens in the collimator was replaced with a pin hole of diameter 2 mm. This was done to ensure that the incident laser beam passes through the center of the spectrometer symmetrically. The objective of the telescope was also removed.

(c) A pair of polarizer and analyzer (Make: Melles Griot) were used for controlling the intensity of the laser beam as we were observing the rainbow and the direct beam through the telescope for measuring the angles.

(d) An Abbe's Refractometer with a least count of 0.001 (Make: Optiregion [7]) as shown in Figure 7 (a) was used to measure the refractive index μ of the acidic solution. This refractometer measures the refractive index of the liquid placed between two glass prisms. Light source is focused at the bottom of the illuminating prism. The refractometer is first calibrated using plain water. After calibration, the water was wiped using soft, splinter-free tissue paper. Then the acidic solution was placed and the refractive index measured by turning the scale knob to get a clear interface between dark and bright regions. The crosswire is then moved to the interface and the value of the refractive index is noted.

(e) A pH meter (Make: Equiptronics, Model: EQ-614A [8]) as shown in Figure 7 (b), was

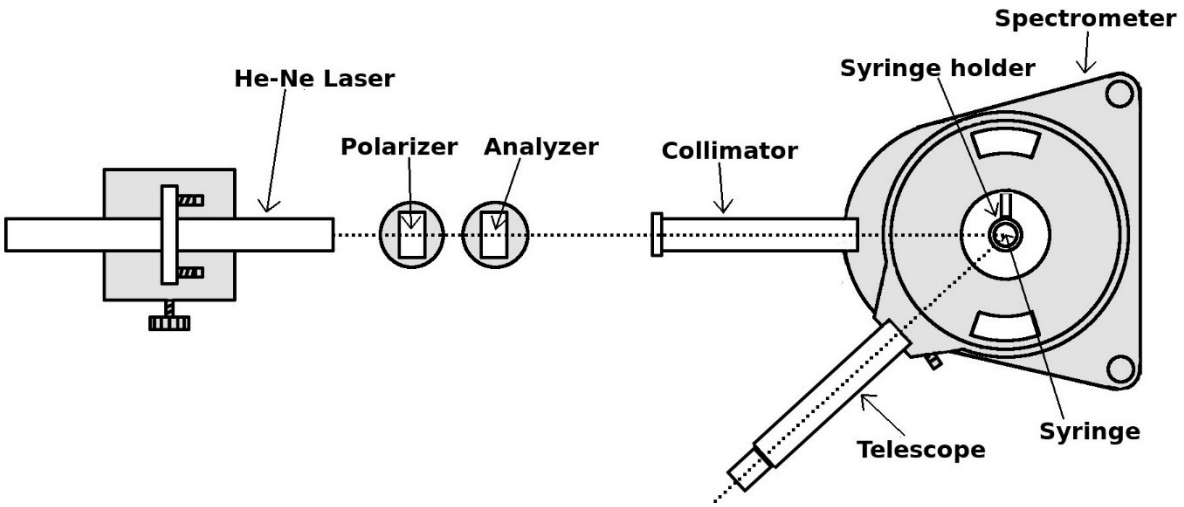

used along with its probe to measure the value of pH of the solution used to study the rainbow angle for each case.

Figure 5: Schematic diagram (top view) of the experimental setup

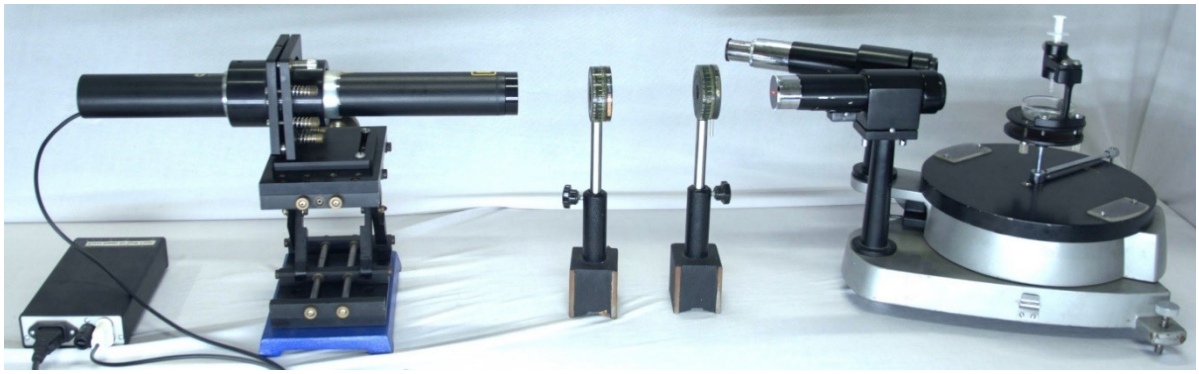

Figure 6: Photograph (oblique view) of the experimental setup

(a)

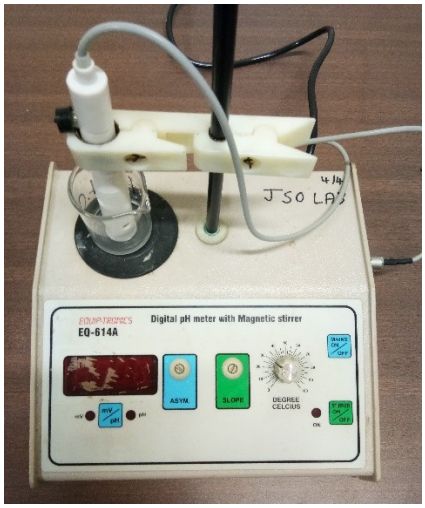

(b)

Figure 7: Photograph of the Abbe's refractometer (a) and the pH meter (b) used in this study

4. OBSERVATIONS AND MEASUREMENTS

The following process was used to collect the required experimental data. First the distilled water was taken in a beaker. Using buffer solutions of pH 4.0, 7.0 and 9.2, the measurement probe of the pH meter was calibrated. Then the probe was washed and placed in the beaker. Using micropipette, a few drops of sulfuric acid (H_2SO_4) (whose concentrated solution was 98% wt./wt.) were added in the beaker and the solution was stirred. Then, a 2 mL syringe was rinsed with the solution in the beaker. A sample of the solution was taken in the syringe and the syringe was mounted on the syringe holder. The laser was switched ON and the intensity of light was reduced using a polarizer and analyzer and then direct beam angle was noted. Now, a pendent drop was formed at the center of the line of the laser by carefully pressing the piston of the syringe. The telescope of the prism spectrometer was moved to the positions where rainbows were forming. The intensity of the laser beam was varied using an analyzer such that the width of the rainbow was reduced and the angle of the first bright fringe was noted for both the orders. We thus measured the total angle of deviation φ_1 and φ_2 for the acidic solution made using sulfuric acid.

Now syringe was taken out and a few drops from it were placed in the Abbe's refractometer and the refractive index μ of the solution was measured. Each time the prism surface inside the refractometer was cleaned using isopropanol and allowed to dry. Also, the value of pH of the solution in the beaker was measured using a pH meter. This entire process was repeated for several solutions with pH varying from 7.0 to 0.0. Further, the entire process was repeated for nitric acid (HNO_3) whose concentrated solution was 70% (wt./wt.).

Figure 8 (a) gives the angular positions of the first (on right) and second (on left) order rainbows as seen from top of the syringe mount, and (b) gives the first bright fringe (which is used for the measurement of the angle of deviation) and interference fringes as observed through the telescope for both the orders. These interference fringes are observed because of the path difference introduced between the emerging rays due to the finite width of the laser beam which is incident on the drop around a particular angle of incidence [2] for each order.

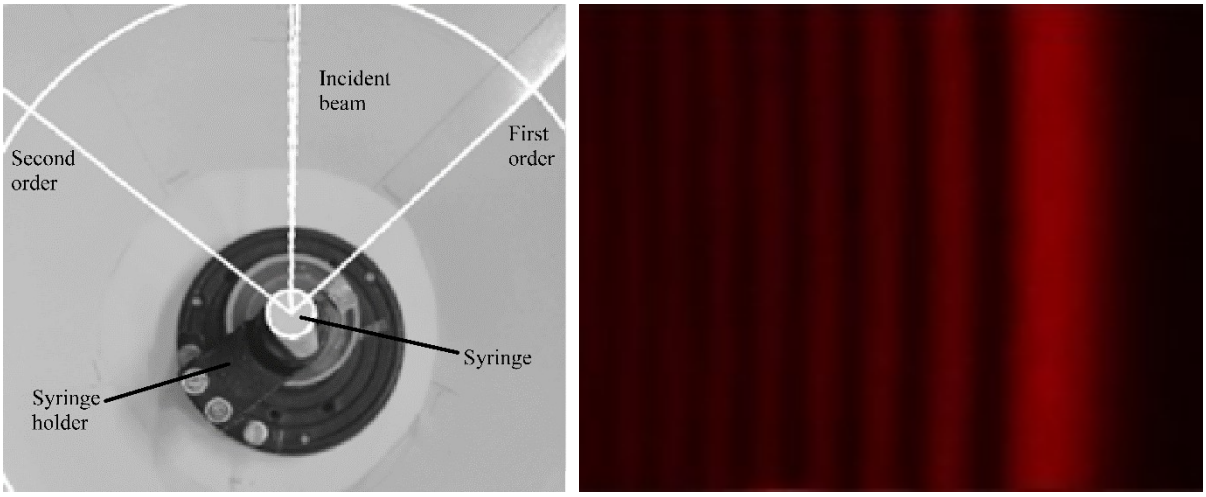

(a) (b)

Figure 8: (a) Angular positions of the first and second order rainbow from top of the syringe, and (b) the interference fringes as observed through the telescope

5. DATA AND RESULTS

Table 1 and Table 2 shows the data collected for the first and second order rainbows for the acidic solutions made using H_2SO_4 and HNO_3. Here, we give the data for measured values pH, refractive index μ and the values of total angle of deviation φ_1 and φ_2 measured using a spectrometer, for 10 measurements performed. Further, using Equation (1) and the experimentally measured value of refractive index μ, we have calculated the theoretically expected values of deviation φ_1 and φ_2. These values are also given in the tables. Note that the telescope focuses at the center of the spectrometer table, since the final rays come out from the surface of the drop which is slightly off-center of the spectrometer table, hence the measured angle of deviation was corrected for this error.

Table 1: Data collected for first and second order rainbow for solutions made with H_2SO_4

Sr. No.	pH	Refrac-tive index (μ)	For first order ϕ_1 /(º)		For second order ϕ_2 /(º)	
			Calculated	Measured	Calculated	Measured
1	7.00	1.332	137.776	137.711	230.628	230.849
2	5.36	1.332	137.776	137.757	230.628	230.850
3	4.86	1.331	137.630	137.762	230.365	230.780
4	3.15	1.332	137.776	137.854	230.628	230.790
5	2.61	1.332	137.776	137.917	230.628	230.706
6	2.08	1.332	137.776	137.854	230.628	230.823
7	1.48	1.333	137.922	137.806	230.891	230.901
8	1.03	1.333	137.922	137.972	230.891	231.083
9	0.52	1.335	138.212	138.260	231.414	231.599
10	0.00	1.340	138.929	138.913	232.709	232.923

Table 2: Data collected for first and second order rainbow for solutions made with HNO_3

Sr. No.	pH	Refractive index (μ)	For first order ϕ_1 / (°)		For second order ϕ_2 /(°)	
			Calculated	Mea-sured	Calculated	Measured
1	7.00	1.332	137.776	137.734	230.628	230.734
2	6.10	1.332	137.776	137.884	230.628	230.417
3	4.05	1.332	137.776	137.628	230.628	230.857
4	3.63	1.332	137.776	137.756	230.628	230.769
5	3.02	1.332	137.776	137.642	230.628	230.817
6	2.03	1.332	137.776	137.862	230.628	230.894
7	1.36	1.333	137.922	137.744	230.891	230.927
8	0.91	1.333	137.922	137.908	230.891	231.260
9	0.58	1.333	137.922	138.040	230.891	231.273
10	0.05	1.337	138.500	138.110	231.934	232.241

We plotted a graph of angle of deviation φ_1 and φ_2 versus pH for both the acids as shown in Figure 9 and 10.

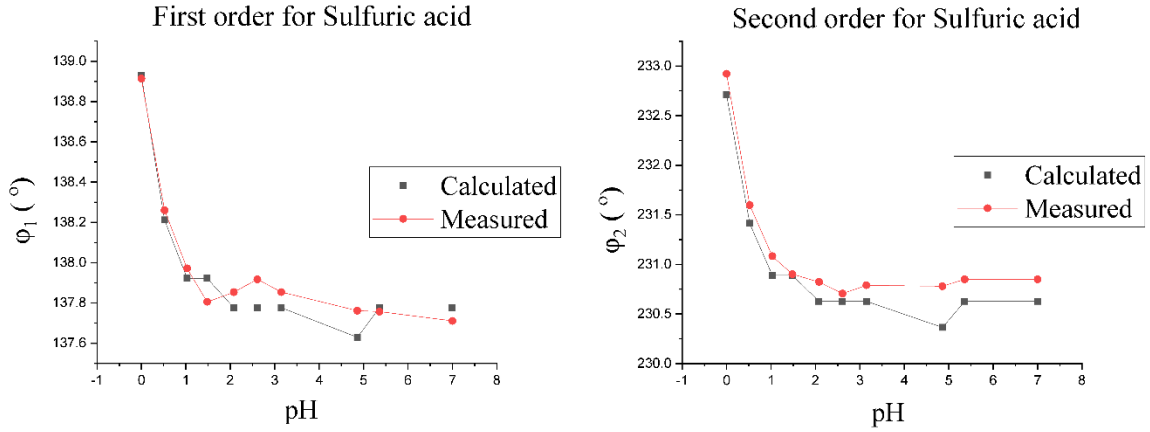

Figure 9: Plots of angle of deviation φ_1 and φ_2 versus pH for the sulfuric acid (H_2SO_4)

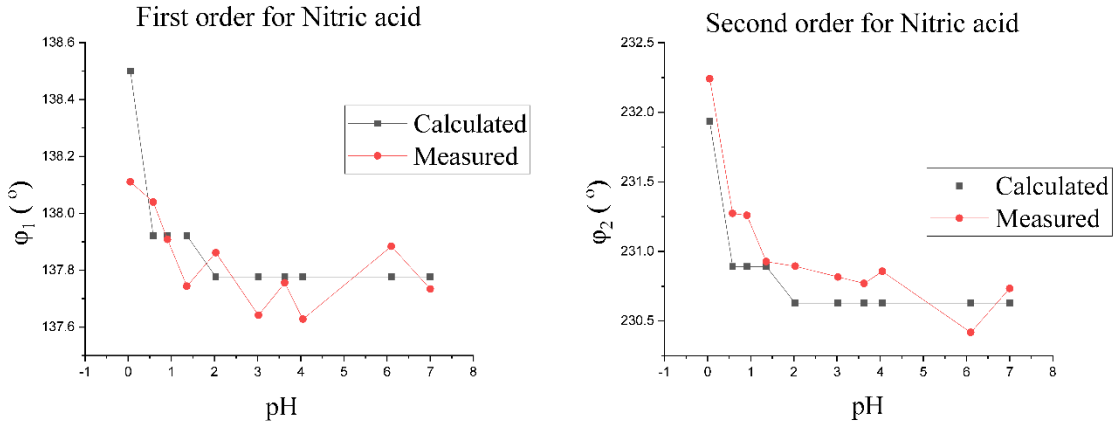

Figure 10: Plots of angle of deviation φ_1 and φ_2 versus pH for the nitric acid (HNO_3)

From the data shown in Table 1 and 2, we calculated the difference in the measured angle of deviation and the angle of deviation calculated from the measured value of the refractive index and Equation (1). Table 3 shows this data for the acidic solutions made with both the acids.

Table 3: Difference in the angle of deviation

For acidic solution made with	Calculated difference for		Measured difference for	
	first order	second order	first order	second order
H_2SO_4 (pH 7.00 to 0.00)	1.153°	2.081°	1.202°	2.074°
HNO_3 (pH 7.00 to 0.05)	0.724°	1.306°	0.376°	1.507°

6. CONCLUSION

We studied the rainbow formation in a single pendent drop of acidic solution in a laboratory set-up and measured the variation of the angle of deviation of the rainbow with the value of pH of the solution of the drop. It was observed that for sulfuric acid, as the pH varied from 7.0 to 0.0, the angle for the first order rainbow varied from 137.711° to 138.913° and for the second order from 230.849° to 232.923. For nitric acid, the angle for first order rainbow varied from 137.734° to 138.110° and for the second order from 230.734° to 232.241, for pH varying from 7.0 to 0.05. Our results show that there is relatively small change in the rainbow angle with variation of pH of the acidic solution of the drop in the typical range for the acid rain (pH of about 4.0 to 5.5). However, strong acid rains can be identified by making simple observations of rainbow angle in the sky. Further, even within the normal range of acidity, with accurate measurements of rainbow angle, one may be able to detect acid rain and get an estimate of the acidity or pH remotely.

ACKNOWLEDGEMENTS

We acknowledge the support of the Department of Atomic Energy, Govt. of India, under Project Identification No. RTI4001. We are also grateful to the National Initiative on Undergraduate Science (NIUS) at the Homi Bhabha Centre for Science Education, TIFR, Mumbai, India, for providing the required facilities and funding for the study. The authors are thankful to the NIUS (Physics) laboratory staff for all their help and support.

REFERENCES

[1] G. E. Likens, Acid Rain, *Fundamentals of Ecosystem Science*, Elsevier Inc., pp. 259-264, 2013.

[2] J. D. Walker, Multiple rainbows from single drops of water and other liquids, *American Journal of Physics,* Vol. 44, No. 5, pp. 421-433, May 1976.

[3] V. H. Veley and J. J. Manley, The Refractive Indices of Sulphuric Acid at Different Concentrations, *Proceedings of the Royal Society of London, Series A,* Vol. 76, No. 512, pp. 469-487, 13 September 1905.

[4] V. H. Veley and J. J. Manley, Some Physical Properties of Nitric Acid Solutions, *Proceedings of the Royal Society of London,* Vol. 69, pp. 86-119, 1901.

[5] Rajesh B Khaparde and H C Pradhan, *Training in Experimental Physics through Demonstrations and Problems*, Penram International Publishing (India) Pvt. Ltd., pp. 221-238, 2009.

[6] Desmos Graphing Calculator, https://www.desmos.com/calculator

[7] http://www.optiregionindia.in/

[8] http://equiptronics.com/analyticalpage/PH_meter.php

OBITUARY

Prof. Steven Moszkowski

Prof. Steven Moszkowski passed away on December 11, 2020. The lifespan of Prof. Steven Moszkowski almost overlapped the advent of Nuclear Physics as a subject in 1940s up to the present time. He has enriched the subject by his profound contributions for almost 70 years. His earliest work in 1950s on the study of the saturation properties of nuclear matter known as MS separation method (Moszkowski and Scott) was a landmark fundamental contribution. The important problem of the incompressibility of nuclear matter was recalculated by him and his collaborators and was found to be 290MeV, significantly different from the accepted value of 230MeV. During his later years, he was deeply engrossed in solving the problem of saturation properties at a fundamental level using the 3-body force. He passed away before he could see the solution of this perennial problem in nuclear physics.

Prof. Moszkowski was deeply associated with Student Journal of Physics (SJP) as a member of its International Advisory Board. Being a first-rate teacher and researcher in Physics all along his life, welfare of students, their cultivation of innovation and creativity was close to his heart. His passionate advice and suggestions to SJP for its development have greatly helped its progress in its formative period. His demise is a great loss to SJP.

STUDENT JOURNAL OF PHYSICS

Volume 8 **Number 3** **2021**

CONTENTS

ARTICLES